Computers and Chemical Engineering 163 (2022) 107816

Contents lists available at ScienceDirect

Computers and Chemical Engineering

journal homepage: www.elsevier.com/locate/compchemeng

A novel time discretization method for solving complex multi-energy system design and operation problems with high penetration of renewable energy

Lukas Weimann, Matteo Gazzani*

Copernicus Institute of Sustainable Development, Utrecht University, 3584 CS Utrecht, the Netherlands

ARTICLE INFO

Article history:
Received 8 November 2021
Revised 9 February 2022
Accepted 20 April 2022
Available online 10 May 2022

Keywords:
MILP
Time discretization
Energy system model
Renewable energy
Optimization

ABSTRACT

Modelling and optimising modern energy systems is inherently complex and often requires methods to simplify the discretization of the temporal domain. However, most of them are either (i) not well suited for systems with a high penetration of non-dispatchable renewables or (ii) too complex to be broadly adopted. In this work, we present a novel method that fits well with high penetration of renewables and different spatial scales. Furthermore, it is framework-independent and simple to implement. We show that, compared to the full time discretization, the proposed method saves >90% computation time with <1% error in the objective function. Moreover, it outperforms commonly used methods of modelling through typical days. Its practical usefulness is demonstrated by applying it to a case study about the optimal hydrogen production from renewable energy. The increased modelling fidelity results in a significantly cheaper design and reveals operational details otherwise hidden by typical days.

1. Introduction

Energy system design and optimisation, from the design of chemical plants to the planning of national infrastructures, has always been a discipline of utmost importance. The emergence of renewable energy technologies, widespread distributed energy generation, and the pressure to timely decarbonize the energy sector to limit global warming brought energy systems optimisation to a new level of difficulty, and therefore put it in the spotlight of an even wider community of researchers. In this context, rigorous mathematical analysis allows not only to outline decarbonization pathways important for policy makers nowadays but also to facilitate the understanding of how technologies interact, need to develop, and how synergies can be exploited. While the current work is focused on multi-energy systems, it is worth highlighting that the increasing volatility of energy supply is also reflected in other related research fields. Representative examples are Mitra et al. (2012), who modelled and optimised transitions in the dynamic operation of gas separation and cement plants for varying electricity prices, Čuček et al. (2014), who optimised supply chains for biofuels such as bioethanol, biodiesel, or Fischer-Tropsch diesel based on multiple periods, or Peng et al. (2021), who studied different thermochemical energy storage systems in concentrated solar plants and developed process models for the optimisation of their design and operation.

When dealing with multi-energy system optimisation, and depending on the purpose of the analysis, four different dimensions of complexity need to be balanced: technology detail, time, space, and uncertainties. Despite Moore's law still holding up, even today computational resources do not allow to solve models with high level of detail in all complexity dimensions in a reasonable amount of time, e.g. multi-year planning considering hourly resolution (and associated uncertainties), detailed and often nonlinear technology descriptions, and multi-node spatial resolution. Priesmann et al. (2019) tried to assess the impact of technology, space, and time complexity domains and suggested that a reduction in overall complexity should start in the technical domain, followed by time and lastly space, in order to maintain accuracy. Wirtz et al. (2021) analysed the impact of technology complexity and also found that a certain extent of simplification can be achieved without significant loss of accuracy. For uncertainties, treated with either robust or stochastic optimisation, tailor-made methods that aim at embedding them into the other three levels of complexity are often used (Grossmann et al., 2015; Pilpola and Lund, 2020; Chen et al., 2021). However, generalised guidelines can easily lead to large errors; as also highlighted by

* Corresponding author.
E-mail address: m.gazzani@uu.nl (M. Gazzani).

https://doi.org/10.1016/j.compchemeng.2022.107816

Nomenclature

MILP	Mixed integer linear programming
NDRES	Non-dispatchable renewable energy conversion technologies
ECT	Energy conversion technology
M-THS	Time-hierarchical solution method
M-TD	Typical design days method (including networks)
M-TDNW	Typical design days method (excluding networks)
M-REF	Reference method
LHV	Lower heating value
$\mathbf{A}$	constraint matrix for continuous variables
$\mathbf{B}$	constraint matrix for binary variables
$\mathbf{b}$	constant term vector of MILP
$\mathbf{C}$	constraint matrix for integer variables
$\mathbf{d}$	cost vector for continuous variables
$\mathbf{e}$	cost vector for binary variables
$\mathbf{f}$	cost vector for integer variables
$\mathbf{x}$	continuous variable vector
$\mathbf{y}$	binary variable vector
$\mathbf{z}$	integer variable vector
S	installed capacity
$P^{\max}$	maximum output power
F	input power or fuel
N	total number of hierarchy layers
x	technology installation decision
u	technology operation decision
T^{amb}	ambient air temperature
Q	thermal output power
N^{on}	number of units operating
T	total number of time intervals
M	total number of nodes
v^{in}	cut-in wind speed
v^{out}	cut-out wind speed
v^{r}	rated wind speed
A	available area
U	imported energy
L	end-user demand
J	costs
d	distance
G	installed network capacity
P	generated power
a	annuity factor
p	price of energy carrier
e	emission factor of energy carrier
max	maximum
min	minimum
PV	photovoltaic
ST	solar thermal
S	solar irradiance
W	wind
c	costs
e	emissions
NW	network
T	technology
O	operation
$\mathcal{O}$	objective function
$\mathcal{E}$	objective function error
α	performance coefficient
β	cost coefficient
γ	fitting parameter (electrolyzer model)
δ	minimum flow or input as a fraction of the installed capacity
Λ	non-weather input data, e.g. energy demands, prices, or resource availability
λ	self-discharge coefficient
θ	weather input data, e.g. solar irradiance or wind speed
σ	length of time instance
ζ	size coefficient
ϕ	mass ratio
ρ	efficiency ratio
κ	network losses
ψ	network flow
χ	maintenance cost factor
n	hierarchy layer/stage
t	time
i	technology or running index of sum
k	type of fuel
m	node
j	type of network or energy carrier
z	segment of piecewise-linear model
$\mathcal{T}$	Set of time instances
$\mathcal{N}$	Set of hierarchy layers
$\mathcal{M}$	Set of nodes
$\mathcal{I}$	Set of technologies
$\mathcal{J}$	Set of energy carriers
$\mathbb{R}$	Real Numbers
$\mathbb{N}$	Natural Numbers including zero

Priesmann et al. (2019), the model complexity needs to fit the research question.

Traditionally, research used to focus on one or two dimensions while drastically simplifying the others. For example, scenario analyses and long-term planning use time horizons of several decades but limit the temporal and spatial granularity and technology detail significantly. On the other hand, detailed process modelling is often limited to steady state analyses or short time horizons for specific dynamic behaviours. More recently, an overlap between those two extremes emerged, which aims at bringing the complexity domains together at sufficient detail. An archetype of such analyses is energy system design considering one year at high temporal resolution and detailed technology models, which are translated into linear models for use in mixed integer linear programming (MILP) optimisations. Although the time horizon is already limited, methods to simplify the temporal domain are still required due to the high resolution, most often hourly, which drastically increases the number of decision variables. This is especially true if weather and demand profiles for different locations are considered to analyse spatially resolved systems including renewable energy technologies. The methods most frequently used for temporal simplification can be assigned to one of three groups: (i) rolling horizon, (ii) time aggregation, and (iii) multi-scale models. Each of these approaches have benefits and drawbacks, and the decision on which is best to use depends on the research question and case study.

The rolling horizon method considers a limited time interval, e.g. one week, which 'rolls' on until a full year (or any other desired time horizon) is analysed. To ensure continuity between the intervals, some overlap between the previous and the next interval is considered. This method is mainly used for the optimisation of operation as exemplified by Marquant et al. (2015), who report computation time savings of more than a factor 10 for optimising the operation of a system of multiple urban energy hubs. Bischi et al. (2019) showed that a rolling horizon can also be combined with constraints on different temporal scales by optimising the operational scheduling of co-generation systems consid-

ering yearly periodicity constraints, cogeneration incentives, and monthly fiscal constraints. With its focus on operation optimisation, the rolling horizon method by itself is not well suited for co-optimisation of design and operation but can be combined with other methods.

Time-aggregation methods aim at reducing the temporal complexity by reducing the number of time instances to be analysed and therefore the number of decision variables. For example, Bakirtzis et al. (2014) used multiple time resolutions for solving unit commitment problems. Starting with a fine time resolution early in the analysed time horizon, periods of increasing length were aggregated for time instances later on the horizon. Vom Stein et al. (2017) also used the idea of varying lengths of aggregated periods. However, they used different measures, e.g. the volatility of input data, to assess which periods require high resolution. More typical for energy system design problems, clustering algorithms are used to derive representative periods of the total time horizon and simplify the design problem. Irrespective of the method, representative periods impose a limit on the operation modes. Therefore, time aggregation methods often require an additional operation optimisation for the full time resolution and constant design - or even multiple iterations to obtain a feasible system. The most commonly used clustering algorithms for this application are k-means, k-medoids, and hierarchical clustering (Kotzur et al., 2018a). While the first two are frequently found and applied in the vast majority of the studies, the latter is less prominent. An interesting application example was provided by Nahmmacher et al. (2016) who implemented time slices based on hierarchical clustering in the TIMES-EU model. A hybrid method was presented by Fazlollahi et al. (2014): they applied k-means in a hierarchical manner, i.e. finding clusters within clusters. More recently, Tso et al. (2020) applied agglomerative hierarchical clustering to optimise renewable power systems with energy storage. The authors highlight the method's ability to preserve the time chronology as crucial for modelling storage technologies.

Several studies compared these three basic clustering methods with similar findings: the best choice depends on the use-case (Kotzur et al., 2018a; Schütz et al., 2018; Pfenninger, 2017). However, independently of the use-case, the analysis of energy systems with high penetration of non-dispatchable renewable energy sources, i.e solar and wind, were identified as particularly challenging and error-prone. This is because (i) wind profiles are hard to cluster due to their volatility, an effect that is amplified by spatially resolved systems in which different wind profiles need to be clustered together, and (ii) inter-period storage, required to dispatch the renewables, cannot be considered using the original approaches. To tackle the latter, Gabrielli et al. (2018a), and later also Kotzur et al. (2018b), proposed a method to couple modelling through typical days, i.e. using representative periods obtained from clustering the original data to represent the full analysis horizon, with seasonal storage. While these improvements increase accuracy when modelling renewable energy systems, they also increase the computation time and a significant error may remain, among other things due to the difficulty of clustering wind profiles. Another pathway to improve the accuracy of time-aggregation methods is the consideration of extreme events. Zatti et al. (2019) proposed *k-MILP*, a k-medoids based clustering algorithm that automatically identifies a defined number of extreme periods, e.g. 20 typical days and two extreme days. It does so by leaving the extreme days as degrees of freedom to the clustering algorithm. In an attempt to minimise the overall error, these degrees of freedom are used for days that show the least similarity with any of the clusters, i.e. extreme periods. A method with a similar goal but different approach was proposed by Teichgraeber et al. (2020), who added slack variables to the operation optimisation and added the day with maximum slack demand to the typical days before iterating over the design optimisation. While neither of those methods were originally developed for systems with a high penetration of renewables, both are useful for such. Most often, time-aggregation methods are applied in two stages: the design is optimised using the aggregated model while the operation is optimised using the non-aggregated profiles. To ensure feasibility, iteration between the two stages is usually needed. The research group around Bardow developed sophisticated methods to improve the computational efficiency of this iterative approach (Bahl et al., 2017; Bahl et al., 2018a; Bahl et al., 2018b; Baumgärtner et al., 2019; Baumgärtner et al., 2020). They introduce features like bounded error in the objective function via convergence criteria and effective treatment of time-coupling constraints, and report computation time savings up to a factor 100. However, the analysed systems are not spatially resolved and consider non-dispatchable renewables only to a limited extent. Furthermore, multiple iterations between the design and operation optimisation remain necessary, which might pose a problem for systems for which the operation problem is hard to solve (e.g. when high renewables penetration, multiple networks, and different storage options come together).

An interesting and rather recent development is the area of multi-scale models, which can be seen as an evolution of time-aggregation methods. Similar to hierarchical clustering, multiple time scales are defined (e.g. a year consisting of typical seasons, which consist of typical days, which consist of typical hours). Nevertheless, where hierarchical clustering is just a means to an end, e.g. finding typical days, multi-scale models utilise all relevant scales, e.g seasonal storage is modelled on a daily scale while renewables are modelled at an hourly scale. The two most significant contributions known to the authors are by Samsatli and Samsatli (2018) and Zhang et al. (2019). Both studies are very similar in their basic idea, but the former presents a more generic framework. The latter, on the other hand, raises an issue that is also important for the present study; it highlights the superiority over models that separate design and operation when treating cases with variable renewables.

In the course of this literature review, no study was found that combines a time horizon of at least one year, hourly temporal resolution, spatial resolution, and technical detail - although some of the aforementioned methodological improvements certainly allow for such analyses. This raises the question why they have not found their way into broader application yet. Presumably, an explanation could be the high complexity and framework specificity of those methods. Furthermore, most studies do not investigate systems with a high penetration of non-dispatchable renewables. In a previous study (Weimann et al., 2021) however, we showed that this is the domain where the accuracy of classical time-aggregation methods suffers the most. Those few studies which consider renewables iterate between design and operation optimisation, which might increase the computation time if the operation optimisation is hard to solve.

To fill this gap, we present a method that (i) is framework independent and simple to implement for researchers and practitioners, (ii) does not necessarily rely on clustering algorithms, (iii) has a limited and a-priori defined number of optimisations, i.e. does not iterate until a convergence criterion is met, (iv) does not separate design and operation optimisation, (v) works for very high penetration of renewables and different spatial scales, and (vi) shows excellent accuracy and drastically reduced computation time.

The rest of this article is structured as follows: in Section 2.1, the general formulation of the mathematical problem and technology models are presented. The remainder of Section 2 covers a detailed description of the proposed time-discretization method, which is the key methodological novelty of this work. The results

in Section 3 consist of two parts. Firstly, the method's performance is assessed and the tuning parameters are discussed. Secondly, we show how the new method allows for a better analysis and produces new insights when applied to a case study of interest. Finally, Section 4 provides a summary of the paper and discusses the limitations of the method.

2. Methodology

2.1. MILP formulation and features

Here, we present a short overview of the multi-energy system optimisation problem. More details can be found in published work (Gabrielli et al., 2018a; Gabrielli et al., 2018b; Gabrielli et al., 2020; Weimann et al., 2021). The energy system design and operation optimisation problem was formulated as an MILP using the energy hub approach (Geidl et al., 2007). The original approach was adapted for spatial resolution by considering a directed graph in which each node constitutes an energy hub with its own input data. The general formulation of the MILP is

$$\begin{aligned} \min_{\mathbf{x},\mathbf{y},\mathbf{z}} \quad & \left(\mathbf{d}'\mathbf{x} + \mathbf{e}'\mathbf{y} + \mathbf{f}'\mathbf{z}\right) \\ \text{s.t.} \quad & \\ & \mathbf{A}\mathbf{x} + \mathbf{B}\mathbf{y} + \mathbf{C}\mathbf{z} = \mathbf{b} \\ & \mathbf{x} \geq 0 \in \mathbb{R}^{N_x}, \mathbf{y} \in \{0,1\}^{N_y}, \mathbf{z} \in \mathbb{N}^{N_z} \end{aligned} \tag{1}$$

where $\mathbf{d}, \mathbf{e}$, and $\mathbf{f}$ are generic cost vectors (the prime-symbol indicates the use of their transpose form) with respect to continuous $\mathbf{x}$, binary $\mathbf{y}$, and integer variables $\mathbf{z}$. $\mathbf{A}, \mathbf{B}$, and $\mathbf{C}$ are their respective constraint matrices and $\mathbf{b}$ is the constant term of the constraints. N represents the dimensions of $\mathbf{x}, \mathbf{y}$, and $\mathbf{z}$ (indicated as subscript). The associated input data are (i) weather data, i.e. wind speed, solar irradiance, and air temperature, (ii) energy demand profiles, (iii) emission factors, prices, and import limitations of energy carriers, and (iv) technology cost and performance parameters. Data sets (i)–(iii) are hourly resolved in the framework, although (iii) was considered to be constant for the cases analysed in the present study, given the limited role of fossil-based electricity therein. Data sets (i) and (ii) are also spatially resolved, and in this work we consider cases both with and without spatial resolution. In the following, the most important equations of the model are summarised for the objective functions, the energy balances, the networks, and the technologies. The reader is referred to the original publications whenever appropriate. In the following equations, $i \in \mathcal{I}$ indicates the technologies, $m \in \mathcal{M}$ indicates the nodes, and $t \in \mathcal{T}$ indicates the time instance. The total number of nodes and time instances are denoted by M and T, respectively.

Objective functions The objective functions of the optimisation problem are the total annual cost of the system, $\mathcal{O}^{\mathrm{c}}$, or the total annual CO_2 emissions, $\mathcal{O}^{\mathrm{e}}$. The former is composed of the annual capital and maintenance cost of technologies J^{T}, the annual capital cost of networks, J^{NW}, and the annual operation cost, J^{O}

$$\mathcal{O}^{\mathrm{c}} = J^{\mathrm{T}} + J^{\mathrm{NW}} + J^{\mathrm{O}} \tag{2}$$

The annual technology costs are expressed as

$$J^{\mathrm{T}} = \sum_{i\in\mathcal{I}} \sum_{m\in\mathcal{M}} \left(\beta_i S_{i,m} + \beta_i'\right)(1+\chi_i) a_i \tag{3}$$

where β and β' represent the variable and fixed cost coefficients, S is the technology size/installed capacity, and χ is a factor accounting for maintenance costs. The equivalent annual investment cost is computed through the annuity factor a, where an interest rate of 10% is considered. The annual operation cost is calculated based on the amount of imported energy U during the year:

$$J^{\mathrm{O}} = \sum_{j\in\mathcal{J}} \sum_{m\in\mathcal{M}} \sum_{t\in\mathcal{T}} p_j U_{j,m,t} \tag{4}$$

where p_j is the price for importing energy carrier j. The emissions are determined solely by the imported energy carriers,

$$\mathcal{O}^{\mathrm{e}} = \sum_{j\in\mathcal{J}} \sum_{m\in\mathcal{M}} \sum_{t\in\mathcal{T}} e_j U_{j,m,t} \tag{5}$$

where e_j is the emission factor of imported energy carrier j. For this to hold true, three assumptions are crucial: (i) no carbon sourcing, e.g. drilling for gas, happens inside the system boundaries, (ii) life-cycle emissions of technologies are neglected, and (iii) all imported energy is consumed in the analysed time period, i.e. no energy is stored in a multi-year fashion.

Energy balance The sum of imported and generated energy must equal the consumed energy for all energy carriers j at all time intervals $t \in \mathcal{T}$

$$\begin{aligned} 0 = & \sum_{\substack{m'\in\mathcal{M} \\ m'\neq m}} \left(\psi_{j,m',m,t}(1-\kappa_j)^{d_{j,m',m}} - \psi_{j,m,m',t}\right) \\ & + \sum_{i\in\mathcal{I}} \left(P_{j,m,i,t} - F_{j,m,i,t}\right) \\ & + U_{j,m,t} - L_{j,m,t} \end{aligned} \tag{6}$$

where P is the energy generation, F the energy stored or consumed by storage or conversion technologies, L the end-user demand, ψ the flow between nodes, and d and κ are the network-specific distance and loss coefficient, respectively.

In case of a copper-plate approach for the networks, i.e. all energy carriers are free to flow without restrictions, the energy balance simplifies to

$$0 = \sum_{m\in\mathcal{M}} \sum_{i\in\mathcal{I}} \left(P_{j,m,i,t} - F_{j,m,i,t}\right) + U_{j,m,t} - L_{j,m,t} \tag{7}$$

Networks The network is described as a directed graph in which the nodes are connected through potentially bi-directional vertices. This graph is characterised by two parameters, namely the connectivity $c_{j,m,m'} \in \{0,1\}$ and distance $d_{j,m,m'} \in \mathbb{R}$ between two nodes m and m' for network j. In the course of this work, each energy carrier has only one associated network, i.e. j also indicates the energy carrier transported. The flow, $\psi_{j,m,m',t}$, from node m to node m' at any time instance t is constrained as

$$\delta_j G_{j,m,m'} \leq \psi_{j,m,m',t} \leq G_{j,m,m'} \tag{8}$$

$$c_{j,m,m'} G^{\min}_{j,m,m'} \leq G_{j,m,m'} \leq c_{j,m,m'} G^{\max}_{j,m,m'} \tag{9}$$

where δ is the minimum flow as a fraction of the installed capacity G. We distinguish two ways of implementing this model, either sizing-and-scheduling or scheduling-only. In the sizing-and-scheduling approach, both the network design and network operation are subject to optimisation, i.e. ψ, c, and G are decision variables. In the scheduling-only approach, only the operation is optimised for a given network, i.e. c is given and $G^{\min} = G^{\max}$. Moreover, a concave, piecewise linear cost-model describing the investment cost J^{NW} was defined to account for existing free capacity

$$J^{\mathrm{NW}}_j = \sum_m \sum_{m'} \left(\sum_z \left[\left(G_{j,m,m'}\beta_{z,j} + \beta'_{z,j}\right) w_{z,j,m,m'} d_{j,m,m'} \right] + c_{j,m,m'}\beta''_j \right) \tag{10}$$

$$\sum_z w_{z,j,m,m'} \leq 1 \tag{11}$$

where β, β', and β'' are cost coefficients, and $w \in \{0,1\}$ is a binary selecting segment z. The bilinearity between G and w was resolved according to Eq. (23). Following this piecewise linear approach, Eq. (9) needs to be adjusted such that

$$G^{\min}_{j,m,m'} = \sum_z G^{\min}_{z,j,m,m'} w_{z,j,m,m'} \tag{12}$$

$$G^{\max}_{j,m,m'} = \sum_z G^{\max}_{z,j,m,m'} w_{z,j,m,m'} \tag{13}$$

As an alternative to the sizing-and-scheduling and scheduling-only network designs, a copper-plate approach can be implemented in which all energy carriers are free to flow between the nodes without restrictions. In this case, Eqs. (8) and (9) become obsolete, and $J^{\mathrm{NW}} = 0$.

Technology cost and performance constraints Two different families of technologies are considered in this work, namely energy conversion technologies (ECTs) and storage technologies. For each technology i, the installed capacity S_i must fall between a minimum and a maximum value, $S_i^{\min}$ and $S_i^{\max}$, respectively

$$S_i^{\min} x_i \le S_i \le S_i^{\max} x_i \tag{14}$$

where the binary variable x_i determines if a technology is installed. $S_i^{\min}$ and $S_i^{\max}$ are decided depending on the case study; however, the interval is typically set very broad intentionally to avoid excluding optimal solutions.

Technology-specific constraints are implemented per family of technology:

Energy conversion technologies. All energy conversion technologies follow the same fundamental logic: the actual power output $P_{i,m,t}$ of technology i at node m and time instance t is constrained by a maximum value $P^{\max}_{i,m,t}$.

$$P_{i,m,t} \le P^{\max}_{i,m,t} \tag{15}$$

This maximum value is determined by the input, which is either a decision variable for dispatchable ECTs or imposed, e.g. by the weather profile, for non-dispatchable ECTs.

- Photovoltaic (PV) and solar thermal (ST) panels: the maximum electric power output of PV panels is described as a function of solar irradiance θ^{S} and ambient air temperature T^{amb}

$$P^{\max}_{m,t} = \eta^{\mathrm{PV}}\left(\theta^{\mathrm{S}}_{m,t}, T^{\mathrm{amb}}_t\right)\theta^{\mathrm{S}}_{m,t} S^{\mathrm{PV}}_m \tag{16}$$

  where η^{PV} is the efficiency calculated as proposed by De Soto et al. (2006). For ST panels, the maximum thermal output power is described as

$$P^{\max}_{m,t} = \eta^{\mathrm{ST}} \theta^{\mathrm{S}}_{m,t} S^{\mathrm{ST}}_m \tag{17}$$

  where the efficiency η^{ST} is a function of the output temperature and considered constant at 0.65 in this work (Gabrielli et al., 2018a). In addition to Eq. (14), PV and ST panels compete for the same available area A

$$S^{\mathrm{PV}}_m + S^{\mathrm{ST}}_m \le A_m \tag{18}$$

- Wind turbines (WT): the maximum power output is calculated as a function of the wind speed θ^{W} and the turbine's performance parameters, namely the cut-in wind speed v^{in}, the rated wind speed v^{r}, the cut-out wind speed v^{out}, and the rated power P^{r} as proposed in Jerez et al. (2015)

$$P^{\max}(\theta^{\mathrm{W}}_{m,t}) = \begin{cases} 0 & \text{if } \theta^{\mathrm{W}}_{m,t} < v^{\mathrm{in}} \\ P^{\mathrm{r}} \frac{(\theta^{\mathrm{W}}_{m,t})^3 - (v^{\mathrm{in}})^3}{(v^{\mathrm{r}})^3 - (v^{\mathrm{in}})^3} & \text{if } v^{\mathrm{in}} \le \theta^{\mathrm{W}}_{m,t} < v^{\mathrm{r}} \\ P^{\mathrm{r}} & \text{if } v^{\mathrm{r}} \le \theta^{\mathrm{W}}_{m,t} < v^{\mathrm{out}} \\ 0 & \text{if } \theta^{\mathrm{W}}_{m,t} \ge v^{\mathrm{out}} \end{cases} \tag{19}$$

  The costs for onshore turbines are solely defined by the turbine price and a constant share of installation cost. For offshore turbines, the costs are a function of turbine price, distance to shore, and water depth. For details about this cost model, the reader is referred to Weimann et al. (2021).

- Polymeric electrolyte membrane electrolysers (PEMECs) and fuel cells (PEMFCs): PEMECs produce hydrogen and oxygen, the latter being neglected in this work, while consuming electricity. Although PEMFCs can produce electricity from natural gas (NG) or hydrogen, we only consider hydrogen as fuel in this work, which has to be produced within the system. The maximum output is described using a piecewise affine approximation as discussed by Gabrielli et al. (2018b)

$$P^{\max}_{m,t} = \alpha_z F_{m,t} + \alpha'_z S_m u_{m,t} \tag{20}$$

$$\delta S_m u_{m,t} \le F_{m,t} \le S_m u_{m,t} \tag{21}$$

  where α_z and α'_z are the coefficients of the zth approximation line segment. For the PEMFC, $P_{m,t}$ and $F_{m,t}$ are the electric power outlet and the lower heating value (LHV) based hydrogen power inlet, respectively, while for the PEMEC they refer to the LHV-based hydrogen power output and the electricity power input, respectively. The binary $u_{m,t}$ is an hourly ON/OFF decision, and δ is the minimum input as a fraction of the installed capacity. The PEMFC is also capable of co-producing heat $Q_{m,t}$

$$Q^{\max}_{m,t} = P^{\max}_{m,t}(\rho - 1) \tag{22}$$

  where ρ is the ratio of first-principle efficiency to electrical efficiency. Further details about the model and its parameters can be found in Gabrielli et al. (2018a).The bilinearity between S and u in Eqs. (20) and (21) is resolved by replacing Su with an auxiliary variable $\tilde{S}$ which is constrained as

$$S^{\min} u_{m,t} \le \tilde{S}_m \le S^{\max} u_{m,t} \tag{23}$$

$$S_m - S^{\max}(1 - u_{m,t}) \le \tilde{S}_m \le S_m \tag{24}$$

  This approach is used to tackle all bilinearities relevant in this work.

- Electrically driven heat pumps (edHP): the maximum thermal power generated is described as

$$P^{\max}_{m,t} = \alpha F_{m,t} f(T^{\mathrm{amb}}_t) + \alpha' S_m u_{m,t} + \alpha'' u_{m,t} \tag{25}$$

$$u_{m,t}(\delta S_m + \gamma) \le F_{m,t} \le u_{m,t}\left(\delta' S_m + \gamma'\right) \tag{26}$$

  where the parameters $\alpha, \alpha', \alpha'', \delta, \delta', \gamma, \gamma'$ are determined by fitting manufacturer data. Further details about the model and its parameters can be found in Gabrielli et al. (2018a).

- Gas turbines (GT): In this work, the gas turbine model presented in Weimann et al. (2019) was used. The maximum power output is

$$P^{\max}_{m,t} = \left(\alpha_k u_{m,t} F_{k,m,t} + \alpha'_k N^{\mathrm{on}}_{k,m,t}\right) f\left(T^{\mathrm{amb}}\right) \tag{27}$$

$$N^{\mathrm{on}}_{k,m,t} \le S_m \tag{28}$$

  where k indicates the fuel used, i.e. hydrogen or natural gas, and N^{on} is the number of turbines operating. The choice of fuel is a design decision, i.e. fuel switching during operation is not possible.

  The heat output $Q^{\max}_{m,t}$ is determined indirectly by deducting the losses in the stack

$$Q^{\max}_{m,t} = F_{k,m,t} - P^{\max}_{m,t} - \phi_k \frac{F_{k,m,t}}{LHV_k} c_p^{\text{flue gas}} \Delta T \tag{29}$$

  where ϕ is the mass ratio between fuel and flue gas and LHV_k is the lower heating value of fuel k.

Energy storage technologies. The energy content $E_{i,m,t}$ of storage technology i at node m and time t can be described as

$$E_{i,m,t} = E_{i,m,t-1}(1 - \lambda) - \lambda' S_{i,m} + \eta^{\mathrm{in}} P^{\mathrm{in}}_{i,m,t} - \frac{1}{\eta^{\mathrm{out}}} P^{\mathrm{out}}_{i,m,t} \tag{30}$$

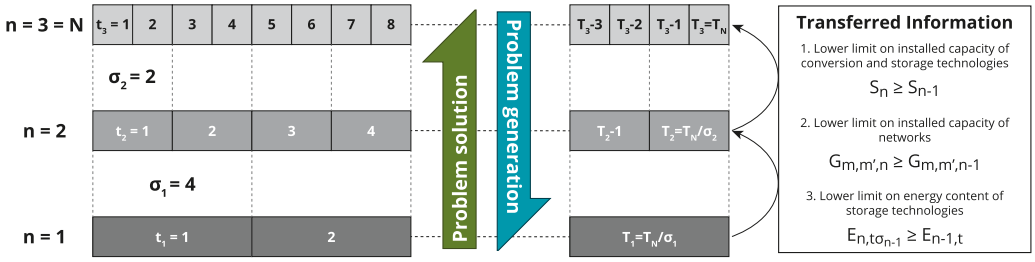

Fig. 1. Graphic representation of the proposed solution method.

where λ and λ' are self-discharge coefficients, and η^{in} and η^{out} are the charging and discharging efficiency, respectively. Furthermore, size and periodicity constraints have to be fulfilled

$$0 \leq E_{i,m,t} \leq S_{i,m} \quad \forall t \in \mathcal{T} \tag{31}$$

$$E_0 = E_T \tag{32}$$

where T is the last time instance of the analysed period. Finally, the maximum charging rate P^{in} and discharging rate P^{out} are limited as

$$P^{\text{in}}_{i,m,t} \leq \frac{S_{i,m}}{\tau^{\text{in}}_i} \tag{33}$$

$$P^{\text{out}}_{i,m,t} \leq \frac{S_{i,m}}{\tau^{\text{out}}_i} \tag{34}$$

where $\tau^{\text{in/out}}$ is the time required to completely charge (in) or discharge (out) the storage medium.

2.2. Time-hierarchical solution method

The method we propose in the current work has its foundations in a common observation in energy system design: the cost of a system designed for average values, e.g. average annual demand, is lower than for a system designed for highly fluctuating values, e.g. hourly demand. The reason for this lies in the volatility of the time series used and can be illustrated by a simple example: an arbitrary energy production unit that follows a sinusoidal operation profile with a maximum of 2 MW, a minimum of 0 MW, and a period length of 0.5 h requires an installed capacity of 2 MW to produce an average of 1 MW. When using an hourly average of the same profile, the technology will be sized at a capacity of just 1 MW, therefore reducing the cost. The same consideration, i.e. averaging temporal profiles reduces the magnitude of peaks and hence the installed capacity, holds for non-dispatchable renewable energy technologies. Additionally, the balancing demands, and therefore storage costs, also reduce for a coarser time discretization. Therefore, the fundamental assumption of our method is that a coarser time-discretization leads to smaller installed capacities of all units, and therefore cheaper system designs, due to a reduction in overall volatility. This feature is used to create a time-hierarchical solution approach where the time-resolution increases with every hierarchy layer, also called *stage* in the present work, as illustrated in Fig. 1. Progressing through the tree, layer $n-1$ provides lower bound constraints for layer n as explained in the following. Note that all constraints presented are resolved by type of technology and location - the respective indices were omitted to improve readability.

Reducing the time resolution of input data. When reducing the time resolution of input data, the method differentiates between profiles that are directly used in the optimisation and profiles which are precursors for data that is used in the optimisation. Energy demands, energy prices, resource availability, and emission factors of imported energy carriers belong to the former category. Weather data input to non-dispatchable technologies belongs instead to the latter category, as they are used in a pre-processing step outside the MILP solution to calculate the maximum power potential of wind and solar power plants at different time instances. This maximum power profile is then directly used in the optimisation itself. In the methodological framework presented in this work, weather profiles are the only example of this category, and in the following we simply differentiate between non-weather input data Λ and weather input data θ.

All time-resolved input data except for weather data are arithmetically averaged to reduce the time resolution according to

$$\begin{aligned} \Lambda_{n,t_n} = & \frac{\sum_i \Lambda_{N,i}}{\sigma_n} \\ & \forall \quad t_n \in \mathcal{T}_n \\ & n \in \mathcal{N}, \quad \mathcal{N} = [1, N] \\ & i \in [(t_n - 1)\sigma_n + 1, t_n\sigma_n] \end{aligned} \tag{35}$$

where n indicates the hierarchy layer, and $\mathcal{N}$ is the set of hierarchy layers with the total number of layers, N. The interval length, σ_n, is the number of subsequent Nth-layer time instances, t_N, used to form one time instance in layer n, t_n (compare with Fig. 1). In the current work, the interval length is constant since a preliminary analysis showed no significant advantage in using variable interval lengths. However, varying the interval length might be beneficial for specific cases, e.g for regions with a significant imbalance between daytime and nighttime. In case of constant interval length, the total number of time instances in the optimisation is given as

$$T_n = \frac{T_N}{\sigma_n} \tag{36}$$

Furthermore, the interval lengths of subsequent layers must fulfil the following condition

$$\frac{\sigma_{n-1}}{\sigma_n} \in \mathbb{N} \tag{37}$$

Opposed to the other time-resolved profiles, weather profiles, θ, are not averaged but carried over between hierarchy layers with their full N^{th}-layer resolution.

$$\theta_{n-1} = \theta_n = \theta_N \tag{38}$$

The resulting dependent profiles, i.e. the maximum power of renewable energy technologies, are averaged according to the relevant time discretization, as explained in detail in the following paragraphs.

Energy conversion technologies. All energy conversion technologies are constrained in size by the previous layer in the form of a lower bound

$$S_n \geq S_{n-1} \tag{39}$$

where S is the installed capacity of any energy conversion technology. Depending on the technology, S can be continuous or integer.

Constraint (39) is the mathematical implementation of the aforementioned fundamental assumption that an increase in volatility of the time series will always lead to greater, or equal, installed capacities. This constraint also tightens constraint (14) on the lower end, hence imposing a positive investment decision for the technology in stage n if $S_{n-1} > 0$.

For the time aggregation in the different stages, conventional dispatchable energy conversion technologies and non-dispatchable renewable energy conversion technologies (NDRES) are treated differently.

As mentioned earlier, the input data for NDRES, i.e. weather profiles, remain at their maximum resolution, no matter the stage. This is an important feature of the proposed method, which leads to a significant improvement compared to methods where a coarser time resolution is adopted irrespective of the technology. In fact, the non-linear input-output correlation for NDRES causes the maximum power calculated from an averaged weather profile to deviate significantly from the value obtained when averaging the maximum power calculated from the original weather profile. Hence, we calculate the maximum power output for one unit in layer n at time instance t_n as

$$P^{\max}_{t_n} = \frac{\sum_i f(\theta_{N,i})}{\sigma_n}, \quad i \in [(t_n - 1)\sigma_n + 1, t_n\sigma_n] \tag{40}$$

where f is the technology specific input-output function, and $\theta_{N,i}$ is the weather profile of layer N, i.e. at original time resolution. Note that this is only possible because the maximum power output is calculated in a pre-processing step outside the MILP solution.

As opposed to NDRES, dispatchable energy conversion technologies do not need modifications when applying this method. As both input power and output power are decision variables, albeit mutually dependent, the models can be applied directly to a problem with reduced time resolution.

Storage technologies. Storage technologies are the only technologies for which the previous stage also imposes constraints on the operation variables, and therefore take a special position in this method. In particular, the energy content or storage level, E, is bound by previous hierarchy layers according to

$$E_{n,t\sigma_{n-1}} \geq E_{n-1,t} \quad \forall \quad t \in \mathcal{T}_{n-1} \tag{41}$$

Furthermore, differentiating between power and energy becomes crucial for time resolutions other than hourly. Therefore, the energy balance described for hourly resolution in Eq. (30) needs to be generalised as

$$E_{t_n} = E_{t_{n-1}}(1-\lambda)^{\sigma_n} + \left(\eta^{\text{in}} P^{\text{in}}_{t_n} - \frac{1}{\eta^{\text{out}}} P^{\text{out}}_{t_n} - \lambda' S\right) \sum_{i=0}^{\sigma_n - 1} (1-\lambda)^i \tag{42}$$

Finally, the installed capacity, S, is also bound by Eq. (39).

Networks. As for energy conversion and storage technologies, the installed capacity of networks has a lower bound imposed by the previous stage

$$G_{m,m',n} \geq G_{m,m',n-1} \tag{43}$$

where $G_{m,m'}$ is the installed capacity for a certain type of network (e.g. pipeline, trucks, electricity grid - index omitted) between nodes m and m'. Similar to storage technologies, networks contribute significantly to the complexity of both the design and the operation problem. This suggests that bounding the operation similar to storage technologies, e.g. applying lower limits on flows, would be beneficial. However, no constraints which improve the performance while ensuring feasibility and accuracy could be formulated. This is a result of the network operation varying significantly between the hierarchy layers.

Objective functions. In a single-objective optimisation, applying bounds on the objective functions throughout hierarchy layers showed only limited effect since the bounds for design variables already imply indirect bounds for the objective functions. However, for multi-objective optimisation (or Pareto optimisations) using the ϵ-constraint or similar methods, i.e. optimising objective **1** while constraining objective **2**, it is imperative to constrain objective **2** at each hierarchy layer

$$\mathcal{O}_{\mathbf{2},n} \leq \mathcal{O}^{\max}_{\mathbf{2},n} \leq \mathcal{O}^{\max}_{\mathbf{2},N} \tag{44}$$

$$\mathcal{O}^{\max}_{\mathbf{2},n} = \mathcal{O}^{\max}_{\mathbf{2},N} \iff n = N \tag{45}$$

Relaxing inequality (44), e.g. by using $\mathcal{O}^{\max}_{\mathbf{2},N}$ to bound $\mathcal{O}_{\mathbf{2},n}$ (if $n \neq N$), can be detrimental for the computation time. Most often however, this cannot be avoided if only $\mathcal{O}^{\max}_{\mathbf{2},N}$ is known. The accuracy is not affected by relaxing inequality (44), as shown in Section 3.3. On the other hand, over-constraining the problem as $\mathcal{O}_{\mathbf{2},n} \leq \mathcal{O}^{\max}_{\mathbf{2},n-1}$ will lead to infeasibility in most cases.

2.3. Method benchmarking

To test the proposed methods under different boundary conditions, three substantially different real-world applications were considered. These feature (i) different energy carriers, (ii) different number of nodes, i.e. different spatial resolution, (iii) different technologies, and (iv) different demand characteristics. All applications were optimised for minimum cost at minimum emissions, i.e. minimising emissions first and applying the found optimum as upper bound in the subsequent cost optimisation.

The first case is an energy system design for a district of the city of Zurich (Switzerland) as analysed in Gabrielli et al. (2018a) (tag 'LZH' for *Local Zurich*). The second case is an energy system design for the campus of Utrecht University (tag 'LC' for *Local Campus*). Both LZH and LC feature electricity and heat demand profiles, as is typical for urban energy system designs. However, the demand profiles vary in magnitude and periodicity. Furthermore, the available space for renewable energy conversion technologies is different. The third case is an energy system design for the Netherlands on a national scale, focused on fulfilling electricity and hydrogen demands (tags N1,N3, and N8 for *national*). Cases LZH, LC, and N1 are not spatially resolved, while cases N3 and N8 are spatially resolved over three nodes and eight nodes, respectively. The networks of N3 and N8 were analysed with different levels of detail: (i) a copper-plate assumption (N3C/N8C), (ii) a scheduling-only network in which the operation is optimised for a fixed capacity (N3S/N8S), and (iii) a network which is optimised for both operation and capacity (N3NW/N8NW). In either case, networks are only considered for electricity and hydrogen. The mathematical formulation of the different networks is described in Section 2.1. Finally, the complexity of each case was further varied by varying the technology portfolio, starting with a simple case (electricity as the only energy carrier, wind turbines and photovoltaics as the only conversion technologies, no storage) and gradually increasing the number of conversion and storage technologies and energy carriers. This results in a total of 38 test cases. To ensure feasibility of the systems, import of electricity entering the system boundaries with an emission factor of 371gCO2/kWhe and costs of 0.034 EUR/kWhe was allowed for, but minimised in the course of the emissions minimisation. An overview of the different cases can be found in Table A.1 in the appendix while Table A.2 summarises the problem size of the different test cases. All case abbreviations used henceforth refer to these tables, unless stated otherwise.

For benchmarking, the proposed method and two other common methods for time discretization were compared against a reference, resulting in four different methods: (i) full hourly resolution as optimal reference (M-REF), (ii) a method using 20 typical design days to model binary-intensive technologies (mostly dispatchable ECTs) and the networks (method M2 presented in

Table 1
Summary of average performance parameters for different methods, relative to the reference method's performance. Note that the reported computation times always include the time for compiling the MILP problem, hence giving the time-hierarchical method an intrinsic disadvantage for very low computation times where the compilation time makes up a significant share of the total computation time.

Ref. comp.	Emission increase [-]			Cost increase [-]			Relative comp. time [-]			Infeasible problems		
time [h]	M-THS	M-TD	M-TDNW	M-THS	M-TD	M-TDNW	M-THS	M-TD	M-TDNW	M-THS	M-TD	M-TDNW
0.01-0.1	<0.001	0.385	<0.001	0.015	0.011	<0.001	0.850	0.880	1.030	1	0	0
0.1-1	<0.001	0.663	0.006	0.012	0.766	0.303	0.195	0.893	0.821	0	2	0
1–10	<0.001	0.540	<0.001	0.008	1.870	0.669	0.073	0.769	0.641	0	0	0
10–100	<0.001	0.253	<0.001	0.007	2.021	0.670	0.082	0.258	0.512	0	0	0

	Problem size	**Continuous variables**	**Integer variables (of which binary)**	**Constraints**
0.01-0.1	median	220,325	8 (0)	341,001
	min/max	64,801/548,660	3/8,643 (0/8,640)	102,873/910,871
0.1-1	median	450,022	149 (128)	811,886
	min/max	144,791/1,454,229	21/21,621 (0/21,600)	257,263/2,562,131
1–10	median	788,414	28,462 (21,856)	1,445,326
	min/max	233,357/2,015,253	71/129,922 (63/43,200)	440,878/3,684,947
10–100	median	1,512,160	87,621 (43,240)	2,887,909
	min/max	466,637/3,066,160	469/259,266 (448/87,856)	880,954/5,856,202

Gabrielli et al. (2018a), in the present work referred to as M-TD), (iii) the same as method (ii) but with networks modelled using the full time resolution instead of design days (M-TDNW), and (iv) the time-hierarchical solution method proposed in the present work using two stages, i.e. $N = 2$ (M-THS). The results were compared for computation time and the optimal value of both objective functions. To avoid confusion by the wide range of values found for the different test cases, results are reported relative to the respective M-REF value. We distinguish between relative values, $\mathcal{O}^{\text{rel}}$, and errors, $\mathcal{E}$

$$\mathcal{O}^{\text{rel}} = \frac{\mathcal{O}^{\text{M-X}}}{\mathcal{O}^{\text{M-REF}}} \tag{46}$$

$$\mathcal{E} = 1 - \frac{\mathcal{O}^{\text{M-REF}}}{\mathcal{O}^{\text{M-X}}} \tag{47}$$

Here, M-X refers to any of M-TD, M-TDNW, or M-THS, and $\mathcal{O}$ also includes the computation time in addition to the objective functions. The definition of $\mathcal{E}$ shown in Eq. (47) was chosen to avoid dividing by zero in case of zero-emission reference designs. Since $\mathcal{O}^{\text{M-REF}} \leq \mathcal{O}^{\text{M-X}}$ always holds for emissions and costs, $\mathcal{E}$ was defined to be zero for cases where $\mathcal{O}^{\text{M-X}} = 0$. As a result, $\mathcal{E}$ always falls between zero and one, reaching a value of one only if $\mathcal{O}^{\text{M-REF}} = 0$ and $\mathcal{O}^{\text{M-X}} > 0$.

Furthermore, a multi-objective optimisation was conducted for case N3S-3 using the ϵ-constraint method to show the performance of M-THS applied to constrained objective functions. In total, four Pareto-optimal points, evenly spaced and spanning the full range from minimum emissions to maximum emissions (i.e. minimum cost) were calculated with M-THS and M-REF.

To test how multi-year analyses can benefit from the proposed method, test cases N8S-3 and N8S-4 (the systems are identical except for the hydrogen demand which is only applied in N8S-4) were extended to two years. For that, weather and demand profiles of the first year were distorted by random noise and applied to the second year. In particular, 5% noise was applied to the demand profiles, 10% noise was applied to the solar irradiance profiles, and 50% noise was applied to the wind speed profiles. Each scenario was optimised for minimum cost at minimum emissions using two and three hierarchy stages. A comparison with M-REF is not possible as it exceeded the computation time limit, but a comparison to the single-year application of M-THS is provided.

All problems were formulated in MATLAB 2018a (The MathWorks Inc., 2018) using the YALMIP-toolbox (Löfberg, 2004), and solved with Gurobi v9.1 (Gurobi Optimization LLC, 2000) on an Intel Xeon Silver 4110 machine (2.10 GHz, 2 sockets, 16 cores, 32 logical processors, 64 GB RAM) assigning 4 logical processors per problem. A time limit of 60 h was applied for each optimisation step (emission and cost optimisation). Cases for which M-REF was infeasible or reached the time limit were neglected in the comparison.

3. Results

3.1. Benchmarking

Figure 2a and b show the error in the emission and cost objective, respectively, for the three compared methods relative to the reference method. In general, time discretization methods introduce an error in both emission and cost objective, albeit more pronounced for the cost objective. The extent of the error introduced also varies widely and ranges from negligibly small errors well below 1% to more than four-fold increases in emissions and eight-fold increases in costs. Contrary to this general observation, M-THS shows excellent accuracy regarding the costs (<1.5% error) and emissions (<0.001% error) over the whole range of test cases. On the other hand, 18 cases with a significant increase in emissions can be observed for M-TD. Eleven of these cases show emissions while the reference had no emissions. However, these errors are solely due to the limitation of operation modes of the networks and vanish using M-TDNW. For the cost objective, M-TD shows up to 8.3-fold increases. Again, some of those errors can be reduced by M-TDNW, but significant increases of up to 2.6-fold remain.

The computation time for the three methods relative to the reference method are shown in Fig. 2c. For reference computation times shorter than 0.1 h, no substantial time savings for either algorithm can be found due to the high share of compilation time. For higher reference computation times, i.e. where really needed, a general trend of decreasing relative computation times can be observed. Nevertheless, a significant amount of test cases shows hardly any decrease in computation time and some even suffer from increased computation time upon application of time discretization methods. Again, M-THS defies this observation and clearly outperforms M-TD and M-TDNW with savings of up to 99% and absence of significant outliers. This is shown more explicitly in Table 1, which reports average values of the data visualised in Fig. 2a–c.

In conclusion, the benchmarking showed the proposed method's superiority, especially for problems featuring computation times longer than 1 h. Here, the method is by a factor 5–10 faster while also keeping the objective function error at

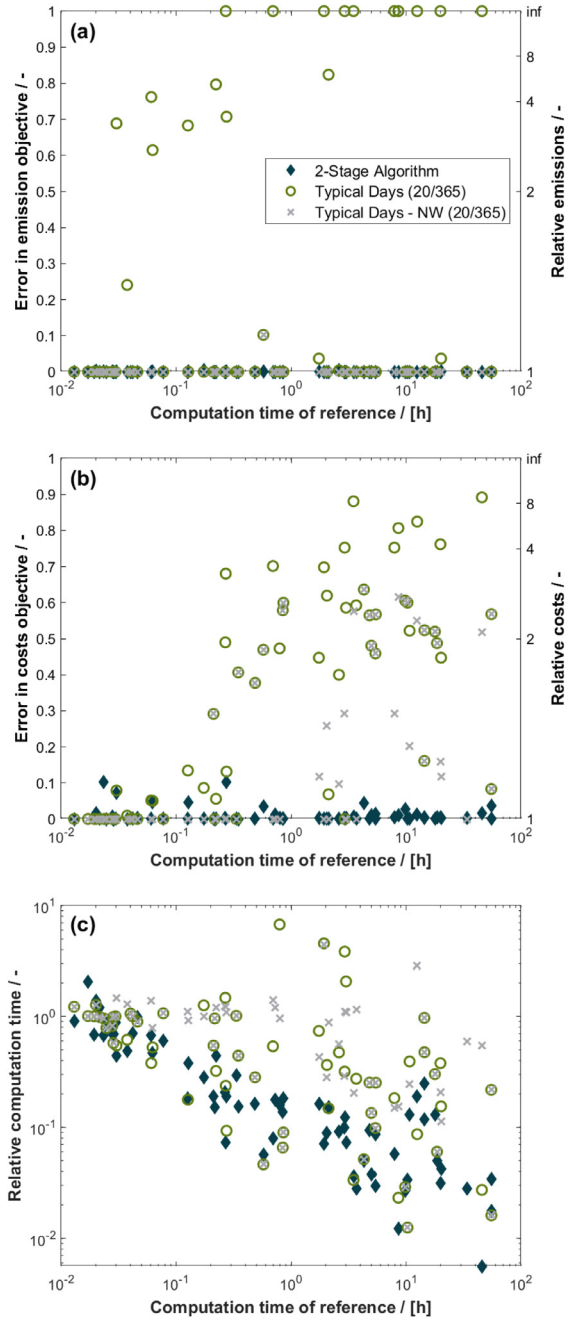

Fig. 2. Comparison of the three evaluated methods against the reference for (a) total emissions, (b) total system costs, and (c) computation time. The definitions of the values shown on the y-axis are reported in Section 2.3. The raw data can be found in Table A.2.

a negligible value ($< 1\%$). It has to be noted at this point that one of the 68 test cases was infeasible using M-THS. This case, together with other limitations of the method, will be discussed in Section 4.1.

3.2. Parameter tuning

The influence of the key parameters of this method, i.e. the number of hierarchy stages N and the interval length σ_n, were investigated first using cases N3S-4 and the more complex N8S-4. To analyse the effect of the interval length, the test cases were optimised for minimum cost at minimum emissions over one year using two hierarchy stages and interval lengths of 12, 8, 6, 4, 3, and 2 h in the first stage. In a second analysis, the effect of the number of stages was investigated by analysing both cases with 1, 2, 3, and 4 stages. Increasing the number of stages automatically introduces different interval lengths. To isolate the two effects, the first-stage interval length was varied as well as shown in Table 2.

Figure 3a and b show the effect of the interval length on the computation time and the objective functions, respectively. For N3S-4, the error in minimum emissions is less than 0.4% for all interval lengths and shows low sensitivity towards this parameter. The minimum cost at minimum emissions are more sensitive to the interval length; however, the maximum error at an interval length of 12 h is still only 1.2%. For interval lengths of 6 h and shorter, the error drops well below 0.5%. The computation time decreases with increasing interval length. This effect is mostly due to savings in the first stage, while the computation time in the second stage is almost constant except for very short interval lengths. In particular, increasing the interval length from 2 h to 6 h, the computation time drops by 50%, while increasing it further to 12 h reduces computation time by only ∼9% additionally. Similar qualitative trends are found for the more complex N8S-4 case (Fig. 3c and d). The error in the cost objective is larger but stays below 5% over the full range, whereas there is no error in emissions (the objective value in the reference case is zero, the relative values were set to 1 for visualisation purposes). The computation time is again dominated by the first stage for short interval lengths and by the second stage for long interval lengths. The effect of increasing the interval length on the computation time is more pronounced than for the simpler N3S-4 case; increasing it from 2 h to 6 h reduces the computation time by 89%, while reducing it further to 12 h reduces the computation time by another 15%. Overall, an interval length of 6 h was identified as a reasonable trade-off between computation time and accuracy. This is despite the sharp increase in the cost objective at 6 h interval length for N8S-4, which is considered a peculiarity of this specific test case.

The effect of the number of stages is shown in Table 2. For both test cases, the interval length in the first stage dominates the error in the objective functions, while the number of stages has only minor effects. This makes sense, since the strongest simplification, which is the first stage by definition, determines the error which is propagated through the stages as a result of the method design. For the computation time, the effect of the number of stages is more complex and can have two outcomes:

i. Adding stages speeds up the problem, as it enables to tighten the bounds step-wise.
ii. For cases where the bounds provided by the first stage are tight already and therefore allow the subsequent stages to solve very fast, the aforementioned benefit is outweighed by the time the additional stages take to solve.

The combination of both effects can be seen for case N3S-4. Starting from two stages with interval lengths of 24 h and 1 h, adding a 6 h stage reduces the computation time by 28%. However, adding another stage with 12 h interval length increases the computation time again by 27%.

Which of the two effects dominates varies and the appropriate number of stages needs to be decided on a case-by-case basis in practice.

3.3. Application examples

Application to Pareto optimisation. The Pareto front shown in Fig. 4 clearly shows the high accuracy of M-THS with respect to M-REF along the whole Pareto front. It is however noteworthy, that the minimum emissions found with M-REF are 0.5% lower than with M-THS. This leads to higher costs at minimum emissions for

Table 2
Effects of the number of stages and interval length on the performance of M-THS for the examples of test cases N3S-4 and N8S-4. All values are relative to the reference reported in the first row.

#Stages	Interval Length	N3S-4			N8S-4		
		Emission	Cost	Comp. time	Emission	Cost	Comp. time
1	1	1	1	1	1	1	1
2	6-1	1.001	1.003	0.161	1.000	1.037	0.024
2	12-1	1.003	1.012	0.133	1.000	1.041	0.020
2	24-1	1.004	1.015	0.197	1.000	1.303	0.017
3	12-6-1	1.003	1.012	0.184	1.000	1.042	0.019
3	24-6-1	1.004	1.015	0.142	1.000	1.304	0.021
4	24-12-6-1	1.004	1.016	0.181	1.000	1.306	0.021

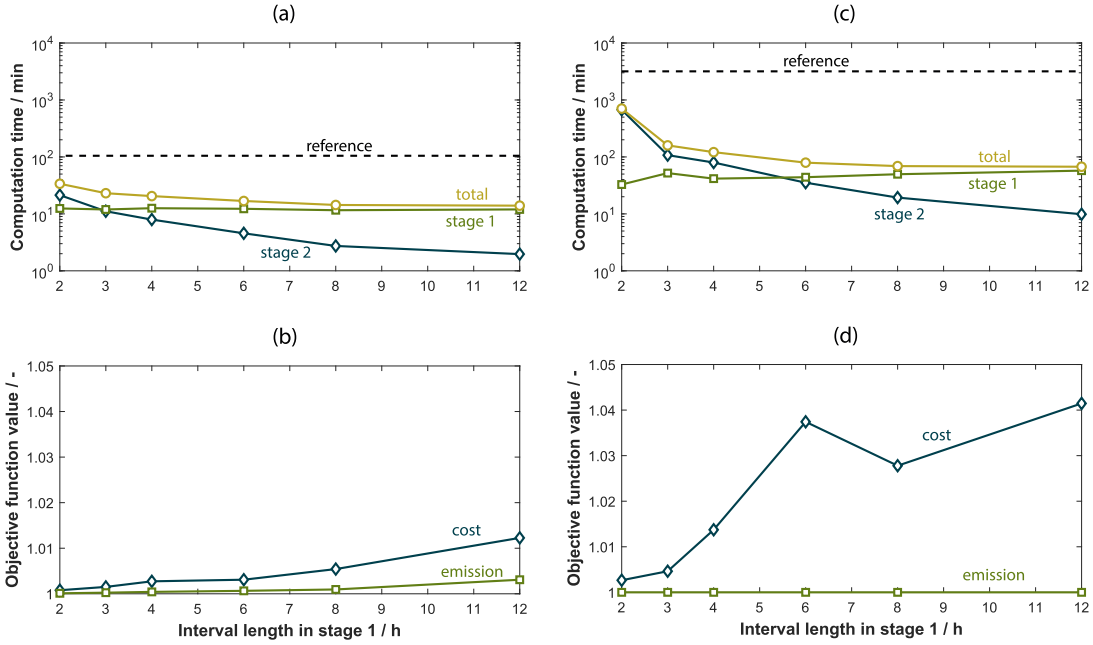

Fig. 3. Effect of interval length on computation time (first row, (a) and (c)) and objective functions (second row, (b) and (d)), for test cases N3S-4 (first column, (a) and (b)) and N8S-4 (second column (c) and (d)). The objective function value is shown relative to the reference case.

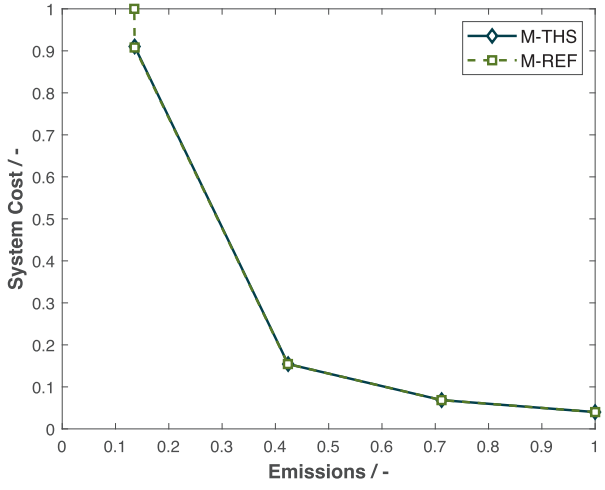

Fig. 4. Comparison of Pareto fronts for case N3S-3 generated using M-THS and M-REF.

M-REF. To identify if the costs for the minimum emissions found by M-THS are accurate, an additional optimisation was conducted with M-REF. In this optimisation, the costs were minimised while having the minimum emissions identified with M-THS as an upper limit. Despite the high accuracy, the computation time for the original four Pareto points is reduced by 82%.

Table 3
Summary of the results of a 2-years analysis of test cases N8S-3 and N8S-4, optimised for minimum cost at minimum emissions.

	Horizon [y]	Int. length [h]	Comp. time [h]	Cost [1010EUR/y]	Emission [tCO_2/y]
N8S-3	1	6-1	1.71	3.963	0
	1	24-6-1	1.43	4.014	0
	2	6-1	7.36	4.164	0
	2	24-6-1	4.79	4.164	0
N8S-4	1	6-1	1.88	7.19	0
	1	24-6-1	1.15	9.04	0
	2	6-1	3.09	7.95	0
	2	24-6-1	4.03	10.53	0

Application to long time periods using multiple stages. The results in Table 3 show that the proposed method allows for co-optimisation of design and operation of systems featuring considerable size and complexity (around 6 million constraints and 3 million variables, of which ~88k integers, for one year) on a 2-year horizon with a computation time of only a few hours. However, since no simplification in the form of typical design periods is used, the problem remains memory intensive for high hierarchy stages. This can lead to intractability on low-memory machines,

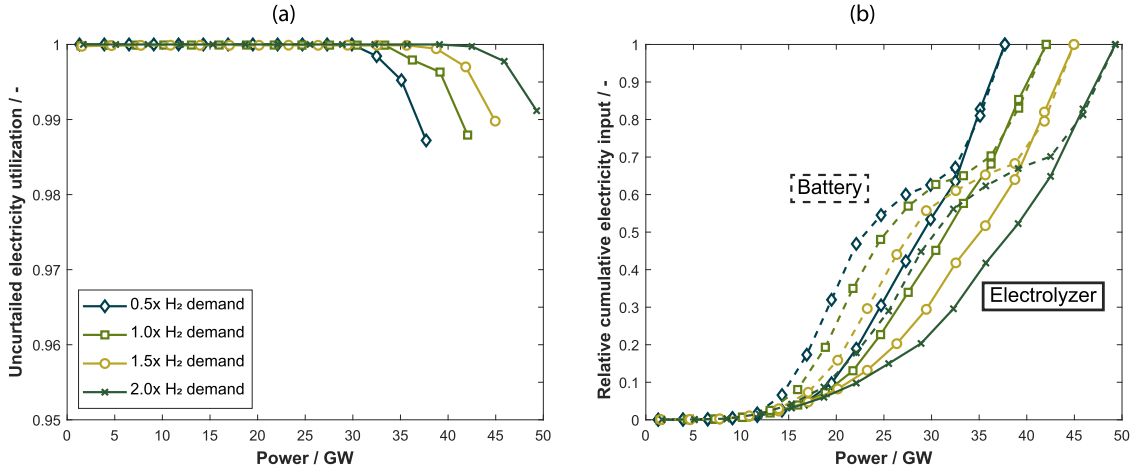

Fig. 5. Results of re-analysing the case presented by Weimann et al. (2021) with M-THS for different H_2 demand scenarios. (a) Utilisation of uncurtailed primary electricity over the power spectrum. (b) Relative cumulative electricity input to batteries and electrolysers (as a proxy for power-to-H_2) over the power spectrum.

and therefore constitutes a potential limitation of this method. Adding additional hierarchy stages can have significant benefits for multi-year analyses, as showcased by the 35% saving in computation time for N8S-3 over two years. However, a prerequisite for this is that the error of the objective function is acceptable, which can already be established on a shorter time horizon; this can be observed by comparing N8S-3 and N8S-4, where the latter shows significant error already for one year. The 2-year analysis of N8S-4 shows that adding stages can also increase the computation time. This effect was discussed in detail in Section 3.2.

3.4. Relevance of time discretization for system design and understanding

Not resorting to design days or other temporal approximations in the final stage of the proposed method not only increases the level of temporal detail of the results but can also lead to different qualitative findings. To demonstrate this, the scenario discussed in Weimann et al. (2021), originally solved using M-TD with 20 typical days to provide a tractable problem, was re-analysed using M-THS. Note that the same scenario was also used as test case N8C in the present study. The savings in computation time were spent on increased spatial resolution (8 nodes in the original study, 15 nodes in the present study) and more detailed network modelling (copper plate in the original study, scheduling-only and sizing-and-scheduling network modelling in the present study, see Section 2.1 for details about the network models)

In the original work, it was shown that the design and operation of power-to-H_2 systems critically depends on the flexibility of these technologies. This was done by varying the number of typical days for a reduced time horizon. While Figure 11b in Weimann et al. (2021) shows that the utilisation of renewable energy increases with increasing operational flexibility (i.e. a higher number of typical days), it was uncertain whether this trend also holds for a longer time horizon, i.e. when seasonal effects come into play. The application of M-THS in the present study shows that the utilisation is indeed significantly higher if no time-aggregation method is used, therefore confirming the finding of the original study. Figure 5a shows how the whole power spectrum is perfectly utilised except for extreme power peaks. Still, even for the latter, the utilisation hardly drops below 99%. Moreover, the original study found that batteries and power-to-H_2 systems take up complementary roles if given the necessary operational flexibility. This finding could also be confirmed on a one year time horizon using M-THS (compare Figure 12 from Weimann et al., 2021 with Fig. 5b in the present work).

Table 4
Key results from applying M-THS to a previous study (Weimann et al., 2021).

	Present study using M-THS	Original study
System cost [MEUR/y]	$1.9 \cdot 10^4$	$3.01 \cdot 10^4$
electrolyser capacity [GW]	23.5	18.4
Fuel cell capacity [GW]	25.0	5.2
H_2 storage capacity [GWh]	4,682	5,681
Battery capacity [GWh]	48.2	576

The advantages of a higher temporal resolution are not limited to operational aspects but can also be found in the designs. Table 4 compares the system costs, battery capacity, and power-to-H_2-to-power capacity found in the original study and the present study. The cost decrease of around 37% clearly shows that the increased flexibility leads to better system designs. In particular, the installed battery capacity decreases by almost 92% while the installed capacities of electrolyser and salt cavern increase only slightly. It should be noted that the original study modelled the battery with full flexibility due to which it compensated for the missing flexibility in the power-to-H_2 technologies. Hence, the strong decrease in installed capacity was to be expected when allowing for more operating modes of the electrolyser. Another significant difference between the two designs is the installed capacity of fuel cells, which increased by a factor 8.7. The small fuel cell capacity in the original study is a result of the decreasing role of H_2 as an electricity storage medium for increasing H_2 commodity demands (see Figure 10 in Weimann et al., 2021). Opposed to this, the analysis using M-THS shows no such decreasing trend but rather a proportional up-scaling of power-to-H_2 capacity with increasing H_2 commodity demand (see Fig. 6). The role of H_2 as electricity storage medium is highlighted in Fig. 6d, which shows that the absolute amount of H_2 used for electricity storage, i.e. the excess production compared to the commodity demand, is rather constant. Conversely, this also implies that the relative amount of H_2 used for electricity storage, compared to the total H_2 produced, is decreasing. While in reality findings like this are influenced by technical constraints, e.g. how electrolysers and fuel cells can be operated, a properly time-resolved modelling framework can help to identify desirable technology features.

Due to the copper-plate approach in the original study, the spatial resolution only affected the system via varying weather pro-

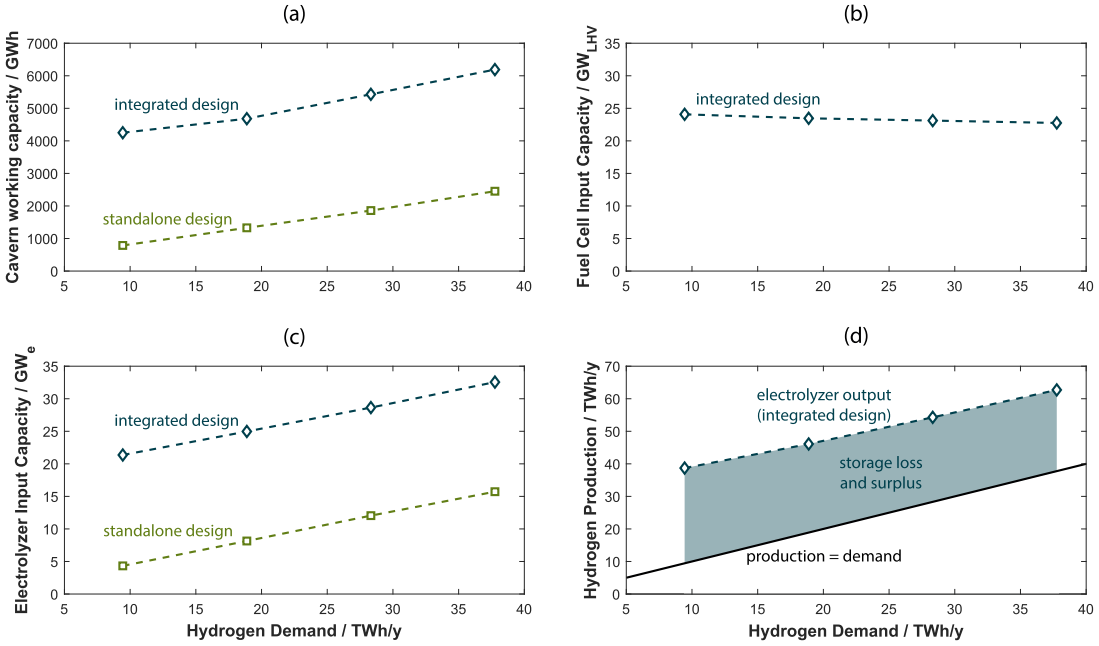

Fig. 6. Sizes of power-to-H_2 technologies as a function of the H_2 demand (re-analysing the case presented in Weimann et al., 2021 with M-THS). (a) Salt cavern (H_2 storage) working capacity (b) Fuel cell input capacity (c) electrolyser input capacity (d) H_2 production.

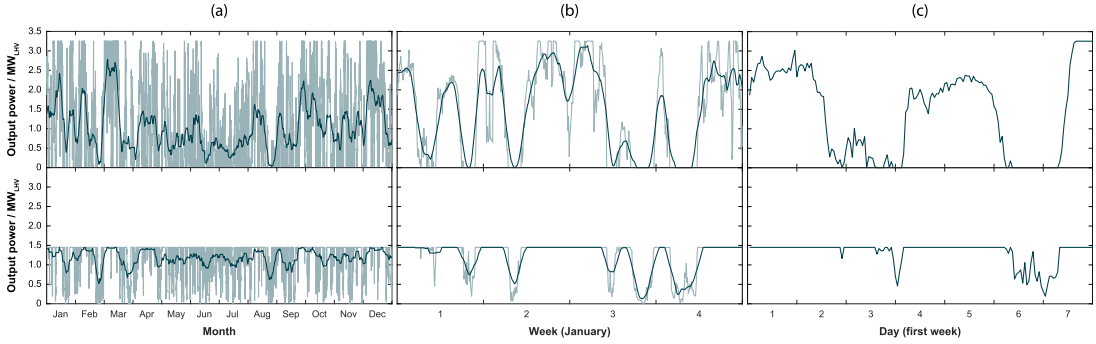

Fig. 7. Production profiles of the electrolysers at the storage site (top) and demand site (bottom). (a) full one year time horizon (b) close-up of the first four weeks of the year (c) close-up of the first week of the year. The light-blue profile is at hourly resolution, the dark blue profile is a moving average of seven days, one day, and one hour for (a), (b), and (c), respectively. (For interpretation of the references to colour in this figure legend, the reader is referred to the web version of this article.)

files. The significantly decreased computation time using M-THS allowed to increase the spatial resolution and model the networks in detail. While the electrolysers were randomly distributed in the original study, they are now limited to two locations. At the storage site, the electrolyser operates in a highly flexible manner following the renewable electricity production since the produced hydrogen can be directly stored (see Figs. 7 and 8). Contrary, at the site where the flat commodity demand is located, the electrolyser preferably operates in steady-state with some disturbances over the year. The electrolyser capacity at the demand site is only 45% of the capacity at the storage site. Considering that some of the H_2 produced at the storage site is also used to supply the commodity demand, the ratio of installed electrolyser capacity agrees with the ratio between storage and commodity demand highlighted earlier (Fig. 6d). It is furthermore noteworthy that the batteries are also installed only at those two sites but with opposing trends in capacity: at the demand site, the smaller electrolyser is combined with the larger battery, while the larger electrolyser at the storage site is combined with the smaller battery. This clearly shows that the steady-state operation periods of the electrolyser at the demand site are facilitated by the battery - an operational feature that is not necessary at the storage site.

Both comparison cases show how the proposed method can contribute to gaining crucial insights otherwise hidden by time aggregation methods. This is especially true for systems with a very high renewable energy penetration, where time aggregation methods can lead to significant deviations from true optimality. An example thereof is the decreasing role of H_2 as electricity storage medium with increasing demand as identified by Weimann et al. (2021), which was shown to be a result of the typical days applied to the model. While the finding in itself is not incorrect, the reason for it - being the reduced operational flexibility of the fuel cell - needs to be acknowledged.

4. Discussion and conclusions

4.1. Method limitations

The method proposed in the current work has been developed with the aim of providing a general and framework-independent method for the solution of complex design and operation optimisa-

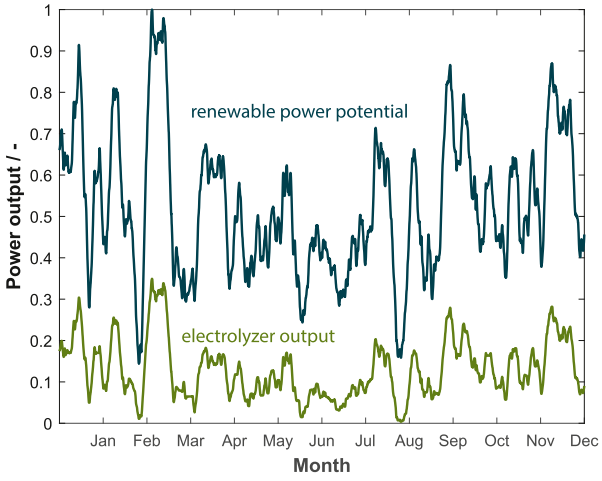

Fig. 8. Total renewable power potential as imposed by the weather profiles and H_2 production (electrolyzer output) at the storage site. Both profiles are relative to the maximum renewable power potential.

tion problems. While this has been mostly achieved, two potential limitations need to be discussed.

Infeasibility for competing technologies. Competing technologies, e.g. two types of wind turbines competing for the same land, can lead to infeasibility in high hierarchy stages. This can happen if the smaller type, i.e. the type with lower power output, is installed to a high extent in an early stage. The increasing temporal resolution of subsequent stages might reveal demand peaks or production valleys which require larger types. However, due to the lower bound imposed by the earlier stage on the small type, the larger type cannot be installed at sufficient quantity. This applies to all technologies which compete for the same land or some other shared resource. The problem can be resolved by applying a lower bound on the amount of shared resource used instead of the size of each single technology. The computation time penalty caused by this looser bound was not quantified in the course of this work.

Intractability for memory intensive problems. The presented method is less suited if the necessity for simplification stems from memory requirements rather than, or in addition to, computation time. An example for this are multi-year analyses. Since the problem is always solved with the maximum time resolution in the last stage of the method, the ultimate memory requirement is not reduced. A potential, yet untested, approach to overcome this limitation is a hybrid of the proposed method and a rolling horizon. The method's parameters should be chosen such that the second-last stage remains tractable. After applying the method's constraints, the last stage can be solved with a rolling horizon.

4.2. Conclusion

In this work, we presented a novel approach to solve intricate MILP energy system design and operation problems for yearly or multi-year time horizons. The method relies on a multi-stage strategy in which the temporal resolution is increased at every stage. The last stage features the maximum resolution provided by the input data, i.e. hourly in the present study. This tackles a commonly known problem of time aggregation methods; they are not reliable for highly volatile systems, e.g. in the case of high renewable energy penetration. Using a vast set of different energy system design and operation optimisation problems, the method was evaluated against optimisations with full time resolution (reference) and benchmarked against a commonly used method relying on typical days. It proved to be both time-efficient (>90% computation time saving compared to the reference) and highly accurate (<1% error in the objective function compared to the reference) and clearly outperformed the typical days method in both domains.

It has to be acknowledged that open literature provides plenty of highly sophisticated time aggregation methods which have not been included in the benchmarking. Therefore, it cannot be ruled out that some of these methods outperform the method proposed in the present work. However, an advantage worth highlighting is the method's simplicity. It does not require clustering algorithms or advanced iterative routines but rather relies on simple averaging of profiles and a set of constraints to transfer information between subsequent stages. Hence, the proposed method is independent of the modelling framework and can be easily applied, therefore having a potentially high impact also outside of academia.

Besides the model formulation, validation, and benchmarking, its practical added value was demonstrated by re-analysing a system for the production of hydrogen from non-dispatchable renewable energy sources the authors discussed in a previous work. The added temporal information provided new insights on the technology operation and system design, and allowed to find a better optimum. Furthermore, it was shown that the increased time efficiency can be used to increase the spatial resolution and the model detail, which results in a better physical representation of the system. Finally, successfully applying the method to a hydrogen production case indicates that it can be used for studying the production of dense chemical energy carriers as well.

Declaration of Competing Interest

The authors declare that they have no known competing financial interests or personal relationships that could have appeared to influence the work reported in this paper.

CRediT authorship contribution statement

Lukas Weimann: Conceptualization, Methodology, Formal analysis, Visualization, Writing – original draft. **Matteo Gazzani:** Conceptualization, Visualization, Supervision, Funding acquisition, Writing – review & editing.

Acknowledgement

ACT ELEGANCY, Project No 271498, has received funding from DETEC (CH), FZJ/PtJ (DE), RVO (NL), Gassnova (NO), BEIS (UK), Gassco AS and Statoil Petroleum AS, and is cofunded by the European Commission under the Horizon 2020 programme, ACT Grant Agreement No 691712.

Appendix A

Table A.1
Summary of test cases.

Tag	ID	Energy carriers	End-user demands	#Nodes	Network	Technologies
LZH	1	electricity	electricity	1	-	WT, PV
LZH	2	electricity	electricity	1	-	WT, PV, battery
LZH	3	electricity, H2	electricity	1	-	WT, PV, battery, PEMEC, PEMFC, H2-storage
LZH	4	electricity, heat	electricity, heat	1	-	WT, PV, ST, battery, edHP, HWTS
LC	1	electricity	electricity	1	-	WT, PV
LC	2	electricity	electricity	1	-	WT, PV, battery
LC	3	electricity, H2	electricity	1	-	WT, PV, battery, PEMEC, PEMFC, H2-storage
LC	4	electricity, H2, heat	electricity, heat	1	-	WT, PV, ST, battery, PEMEC, PEMFC, H2-storage, edHP, HWTS
N1	1	electricity	electricity	1	-	WT, PV
N1	2	electricity	electricity	1	-	WT, PV, battery
N1	3	electricity, H2	electricity	1	-	WT, PV, battery, PEMEC, PEMFC, H2-storage
N1	4	electricity, H2	electricity, H2	1	-	WT, PV, battery, PEMEC, PEMFC, H2-storage
N1	5	electricity, H2, gas	electricity, H2	1	-	WT, PV, battery, PEMEC, PEMFC, H2-storage, GT
N3C	1	electricity	electricity	3	copper-plate	WT, PV
N3C	2	electricity	electricity	3	copper-plate	WT, PV, battery
N3C	3	electricity, H2	electricity	3	copper-plate	WT, PV, battery, PEMEC, PEMFC, H2-storage
N3C	4	electricity, H2	electricity, H2	3	copper-plate	WT, PV, battery, PEMEC, PEMFC, H2-storage
N3C	5	electricity, H2, gas	electricity, H2	3	copper-plate	WT, PV, battery, PEMEC, PEMFC, H2-storage, GT
N3S	1	electricity	electricity	3	capacity limit, no sizing	WT, PV
N3S	2	electricity	electricity	3	capacity limit, no sizing	WT, PV, battery
N3S	3	electricity, H2	electricity	3	capacity limit, no sizing	WT, PV, battery, PEMEC, PEMFC, H2-storage
N3S	4	electricity, H2	electricity, H2	3	capacity limit, no sizing	WT, PV, battery, PEMEC, PEMFC, H2-storage
N3S	5	electricity, H2, gas	electricity, H2	3	capacity limit, no sizing	WT, PV, battery, PEMEC, PEMFC, H2-storage, GT
N3NW	1	electricity	electricity	3	full network design	WT, PV
N3NW	2	electricity	electricity	3	full network design	WT, PV, battery
N3NW	3	electricity, H2	electricity	3	full network design	WT, PV, battery, PEMEC, PEMFC, H2-storage
N3NW	4	electricity, H2	electricity, H2	3	full network design	WT, PV, battery, PEMEC, PEMFC, H2-storage
N3NW	5	electricity, H2, gas	electricity, H2	3	full network design	WT, PV, battery, PEMEC, PEMFC, H2-storage, GT
N8C	1	electricity	electricity	8	copper-plate	WT, PV
N8C	2	electricity	electricity	8	copper-plate	WT, PV, battery
N8C	3	electricity, H2	electricity	8	copper-plate	WT, PV, battery, PEMEC, PEMFC, H2-storage
N8C	4	electricity, H2	electricity, H2	8	copper-plate	WT, PV, battery, PEMEC, PEMFC, H2-storage
N8C	5	electricity, H2, gas	electricity, H2	8	copper-plate	WT, PV, battery, PEMEC, PEMFC, H2-storage, GT
N8S	1	electricity	electricity	8	capacity limit, no sizing	WT, PV
N8S	2	electricity	electricity	8	capacity limit, no sizing	WT, PV, battery
N8S	3	electricity, H2	electricity	8	capacity limit, no sizing	WT, PV, battery, PEMEC, PEMFC, H2-storage
N8S	4	electricity, H2	electricity, H2	8	capacity limit, no sizing	WT, PV, battery, PEMEC, PEMFC, H2-storage
N8S	5	electricity, H2, gas	electricity, H2	8	capacity limit, no sizing	WT, PV, battery, PEMEC, PEMFC, H2-storage, GT
N8NW	1	electricity	electricity	8	full network design	WT, PV
N8NW	2	electricity	electricity	8	full network design	WT, PV, battery
N8NW	3	electricity, H2	electricity	8	full network design	WT, PV, battery, PEMEC, PEMFC, H2-storage
N8NW	4	electricity, H2	electricity, H2	8	full network design	WT, PV, battery, PEMEC, PEMFC, H2-storage
N8NW	5	electricity, H2, gas	electricity, H2	8	full network design	WT, PV, battery, PEMEC, PEMFC, H2-storage, GT

Table A.2
Problem size and benchmark results for all successfully evaluated test cases.

Case	Horizon [d]	Problem size (reference)				Computation time [h]				Emissions [tCO_2/y]				Costs [EUR/y]			
		Cont. variable	Int. variables	Bin. variables	Constraints	M-REF	M-THS	M-TD	M-TDNW	M-REF	M-THS	M-TD	M-TDNW	M-REF	M-THS	M-TD	M-TDNW
LC-1	365	131,404	3	0	205,678	0.017	0.035	0.017	0.017	2848.6	2848.6	2848.6	2848.6	8E+08	8E+08	8E+08	8E+08
LC-2	365	175,204	3	0	293,283	0.022	0.026	0.021	0.021	0	0	0	0	4E+07	4E+07	4E+07	4E+07
LC-3	365	367,928	17,523	17,520	687,493	0.486	0.079	0.137	0.137	0	0	0	0	2E+07	2E+07	3E+07	3E+07
LC-4	365	569,419	35,051	35,048	1,143,052	4.295	0.216	0.222	0.222	0	0	0	0	4E+07	4E+07	1E+08	1E+08
LZH-1	180	64,801	3	0	102,873	0.028	0.020	0.016	0.016	61.644	61.645	61.644	61.644	290,952	290,945	290,952	290,952
LZH-2	180	86,404	3	0	146,078	0.028	0.023	0.023	0.023	41.923	41.973	41.923	41.923	985,031	991,276	985,031	985,031
LZH-3	180	181,448	8643	8640	340,488	0.046	0.046	0.041	0.041	41.923	41.924	41.923	41.923	985,182	988,322	985,182	985,182
LZH-4	180	185,775	8651	8648	366,775	0.574	0.033	0.027	0.027	128.99	129.05	143.7	143.7	694,323	719,687	1E+06	1E+06
LZH-1	365	131,404	3	0	208,693	0.025	0.021	0.019	0.019	128.2	128.2	128.2	128.2	316,818	316,815	316,818	316,818
LZH-2	365	175,204	3	0	296,298	0.020	0.028	0.026	0.026	91.311	91.564	91.311	91.311	1E+06	1E+06	1E+06	1E+06
N1-1	365	183,961	5	0	280,341	0.013	0.012	0.016	0.016	6E+06	6E+06	6E+06	6E+06	8E+10	8E+10	8E+10	8E+10
N1-2	365	227,764	5	0	367,946	0.019	0.013	0.019	0.019	0	0	0	0	7E+10	7E+10	7E+10	7E+10
N1-3	365	420,488	17,525	17,520	762,156	0.211	0.040	0.115	0.115	0	0	0	0	4E+10	4E+10	5E+10	5E+10
N1-4	365	420,488	17,525	17,520	762,156	0.347	0.053	0.154	0.154	0	0	0	0	4E+10	4E+10	6E+10	6E+10
N1-5	365	586,937	105,134	17,528	1,243,991	9.818	0.264	0.285	0.285	0	0	0	0	2E+10	2E+10	6E+10	6E+10
N3C-1	365	341,642	8	0	533,278	0.024	0.016	0.023	0.023	6E+06	6E+06	6E+06	6E+06	5E+10	5E+10	5E+10	5E+10
N3C-2	365	429,248	8	0	708,488	0.042	0.030	0.042	0.042	0	0	0	0	6E+10	6E+10	6E+10	6E+10
N3C-3	365	788,414	35,048	35,040	1,435,583	5.414	0.161	0.533	0.533	0	0	0	0	2E+10	2E+10	4E+10	4E+10
N3C-4	365	788,414	35,048	35,040	1,435,583	4.986	0.189	0.672	0.672	0	0	0	0	3E+10	3E+10	5E+10	5E+10
N3C-5	365	1,147,592	210,266	35,056	2,443,053	18.580	0.925	1.119	1.119	0	0	0	0	3E+10	3E+10	5E+10	5E+10
N3NW-1	180	246,305	71	63	427,329	0.127	0.023	0.022	0.140	3E+06	3E+06	9E+06	3E+06	5E+10	5E+10	5E+10	5E+10
N3NW-2	180	289,511	71	63	513,739	0.695	0.056	0.374	0.973	0	0	250,212	0	6E+10	6E+10	2E+11	6E+10
N3NW-3	180	466,637	17,351	17,343	880,954	45.690	0.258	1.246	24.897	0	0	87,817	0	2E+10	2E+10	2E+11	5E+10
N3NW-4	180	466,637	17,351	17,343	880,954	12.492	2.389	1.083	36.187	0	0	2E+06	0	3E+10	3E+10	2E+11	6E+10
N3NW-1	365	499,385	71	63	866,410	0.274	0.053	0.026	0.301	6E+06	6E+06	2E+07	6E+06	5E+10	5E+10	6E+10	5E+10
N3NW-2	365	586,991	71	63	1,041,620	1.930	0.138	8.793	8.541	0	0	3E+06	0	6E+10	6E+10	2E+11	6E+10
N3NW-1	90	123,185	71	63	214,053	0.030	0.013	0.017	0.044	2E+06	2E+06	5E+06	2E+06	5E+10	5E+10	5E+10	5E+10
N3NW-2	90	144,791	71	63	257,263	0.270	0.020	0.064	0.329	0	0	520,693	0	6E+10	6E+10	2E+11	6E+10
N3NW-3	90	233,357	8711	8703	440,878	3.491	0.126	0.117	0.708	0	0	520,695	0	2E+10	2E+10	2E+11	5E+10
N3NW-4	90	233,357	8711	8703	440,878	8.576	0.105	0.199	1.330	0	0	3E+06	0	3E+10	3E+10	1E+11	7E+10
N3S-1	365	420,491	26	18	708,514	0.037	0.018	0.023	0.048	2E+07	2E+07	2E+07	2E+07	6E+10	6E+10	6E+10	6E+10

(*continued on next page*)

Table A.2 (*continued*)

Case	Horizon [d]	Problem size (reference)				Computation time [h]				Emissions [tCO_2/y]				Costs [EUR/y]			
		Cont. variable	Int. variables	Bin. variables	Constraints	M-REF	M-THS	M-TD	M-TDNW	M-REF	M-THS	M-TD	M-TDNW	M-REF	M-THS	M-TD	M-TDNW
N3S-2	365	420,491	26	18	708,514	0.174	0.049	0.219	0.174	6E+06	6E+06	6E+06	6E+06	1E+11	1E+11	1E+11	1E+11
N3S-3	365	946,112	35,084	35,076	1,786,055	2.610	0.239	1.237	1.462	5E+06	5E+06	5E+06	5E+06	1E+11	1E+11	2E+11	1E+11
N3S-4	365	946,112	35,084	35,076	1,786,055	1.745	0.283	1.291	0.755	1E+07	1E+07	1E+07	1E+07	9E+10	9E+10	2E+11	1E+11
N3S-5	365	1,305,290	210,302	35,092	2,793,525	20.169	0.851	3.114	2.278	1E+07	1E+07	1E+07	1E+07	9E+10	9E+10	2E+11	1E+11
N8C-1	180	440,645	21	0	679,824	0.040	0.029	0.043	0.043	1E+06	0	1E+06	1E+06	5E+10	0	5E+10	5E+10
N8C-2	180	548,660	21	0	895,849	0.077	0.047	0.082	0.082	0	0	0	0	4E+10	4E+10	4E+10	4E+10
N8C-3	180	959,072	43,221	43,200	1,720,999	4.809	0.451	1.217	1.217	0	0	0	0	2E+10	2E+10	4E+10	4E+10
N8C-4	180	959,072	43,221	43,200	1,720,999	5.462	0.473	1.378	1.378	0	0	0	0	2E+10	2E+10	4E+10	4E+10
N8C-5	180	1,408,397	259,266	43,240	2,969,654	55.269	0.974	0.892	0.892	0	0	0	0	2E+10	2E+10	4E+10	4E+10
N8C-1	365	893,525	21	0	1,379,277	0.217	0.033	0.208	0.208	3E+06	3E+06	3E+06	3E+06	5E+10	5E+10	5E+10	5E+10
N8C-2	365	1,112,540	21	0	1,817,302	0.333	0.098	0.338	0.338	0	0	0	0	4E+10	4E+10	4E+10	4E+10
N8C-3	365	1,944,752	87,621	87,600	3,490,492	14.458	3.587	6.881	6.881	0	0	0	0	2E+10	2E+10	3E+10	3E+10
N8C-4	365	1,944,752	87,621	87,600	3,490,492	17.822	2.315	5.380	5.380	0	0	0	0	2E+10	2E+10	4E+10	4E+10
N8C-1	90	220,325	21	0	341,001	0.028	0.019	0.028	0.028	1E+06	1E+06	1E+06	1E+06	5E+10	5E+10	5E+10	5E+10
N8C-2	90	274,340	21	0	449,026	0.030	0.026	0.030	0.030	0	0	0	0	4E+10	4E+10	4E+10	4E+10
N8C-3	90	479,552	21,621	21,600	861,616	0.846	0.116	0.056	0.056	0	0	0	0	2E+10	2E+10	4E+10	4E+10
N8C-4	90	479,552	21,621	21,600	861,616	0.857	0.157	0.077	0.077	0	0	0	0	2E+10	2E+10	5E+10	5E+10
N8C-5	90	704,237	129,666	21,640	1,486,031	10.295	0.345	0.129	0.129	0	0	0	0	2E+10	2E+10	5E+10	5E+10
N8NW-1	180	994,053	469	448	1,817,774	0.222	0.098	0.072	0.267	1E+06	1E+06	7E+06	1E+06	5E+10	5E+10	5E+10	5E+10
N8NW-2	180	1,102,068	469	448	2,033,799	3.006	0.220	6.214	3.283	0	0	0	0	4E+10	4E+10	1E+11	4E+10
N8NW-1	365	2,015,253	469	448	3,684,947	2.118	0.322	0.314	1.860	3E+06	3E+06	2E+07	3E+06	5E+10	5E+10	6E+10	5E+10
N8NW-2	365	2,234,268	469	448	4,122,972	33.752	0.941	67.028	20.080	0	0	0	0	4E+10	4E+10	0	4E+10
N8NW-1	90	497,253	469	448	910,871	0.061	0.041	0.023	0.084	1E+06	1E+06	4E+06	1E+06	5E+10	5E+10	5E+10	5E+10
N8NW-2	90	551,268	469	448	1,018,896	3.685	0.104	1.011	4.235	0	0	0	0	4E+10	4E+10	1E+11	4E+10
N8S-1	180	717,189	149	128	1,263,278	0.127	0.048	0.096	0.117	2E+06	2E+06	0	2E+06	5E+10	5E+10	0	5E+10
N8S-2	180	825,204	149	128	1,479,303	0.794	0.125	5.361	0.766	0	0	0	0	6E+10	6E+10	1E+11	6E+10
N8S-3	180	1,512,160	43,477	43,456	2,887,909	10.736	1.400	4.214	2.628	0	0	0	0	4E+10	4E+10	8E+10	5E+10
N8S-4	180	1,512,160	43,477	43,456	2,887,909	19.899	0.628	7.537	4.128	0	0	345,373	0	6E+10	6E+10	2E+11	7E+10
N8S-1	365	1,454,229	149	128	2,562,131	0.725	0.129	0.359	0.871	5E+06	5E+06	0	5E+06	5E+10	5E+10	0	5E+10
N8S-2	365	1,673,244	149	128	3,000,156	2.926	0.361	11.243	3.244	0	0	0	0	6E+10	6E+10	6E+10	6E+10
N8S-3	365	3,066,160	87,877	87,856	5,856,202	14.431	1.709	14.001	14.001	0	0	0	0	4E+10	4E+10	5E+10	5E+10
N8S-4	365	3,066,160	87,877	87,856	5,856,202	55.124	1.883	12.013	12.013	0	0	0	0	7E+10	7E+10	8E+10	8E+10
N8S-1	90	358,629	149	128	632,855	0.062	0.029	0.033	0.049	2E+06	2E+06	4E+06	2E+06	5E+10	5E+10	5E+10	5E+10
N8S-2	90	412,644	149	128	740,880	0.268	0.055	0.394	0.330	0	0	0	0	6E+10	6E+10	1E+11	6E+10
N8S-3	90	756,160	21,877	21,856	1,445,326	2.051	0.181	0.748	0.577	0	0	0	0	4E+10	4E+10	1E+11	5E+10
N8S-4	90	756,160	21,877	21,856	1,445,326	2.923	0.292	0.930	0.843	0	0	603,913	0	6E+10	6E+10	2E+11	8E+10
N8S-5	90	980,845	129,922	21,896	2,069,741	7.912	0.454	1.451	1.191	0	0	603,913	0	6E+10	6E+10	2E+11	8E+10

References

Bahl, B., Kümpel, A., Seele, H., Lampe, M., Bardow, A., 2017. Time-series aggregation for synthesis problems by bounding error in the objective function. Energy 135, 900–912. doi:10.1016/j.energy.2017.06.082.

Bahl, B., Lützow, J., Shu, D., Hollermann, D.E., Lampe, M., Hennen, M., Bardow, A., 2018. Rigorous synthesis of energy systems by decomposition via time-series aggregation. Comput. Chem. Eng. 112, 70–81. doi:10.1016/j.compchemeng.2018.01.023.

Bahl, B., Söhler, T., Hennen, M., Bardow, A., 2018. Typical periods for two-stage synthesis by time-series aggregation with bounded error in objective function. Front. Energy Res. 5. doi:10.3389/fenrg.2017.00035.

Bakirtzis, E.A., Biskas, P.N., Labridis, D.P., Bakirtzis, A.G., 2014. Multiple time resolution unit commitment for short-term operations scheduling under high renewable penetration. IEEE Trans. Power Syst. 29 (1), 149–159. doi:10.1109/TPWRS.2013.2278215.

Baumgärtner, N., Bahl, B., Hennen, M., Bardow, A., 2019. RiSES3: rigorous synthesis of energy supply and storage systems via time-series relaxation and aggregation. Comput. Chem. Eng. 127, 127–139. doi:10.1016/j.compchemeng.2019.02.006.

Baumgärtner, N., Shu, D., Bahl, B., Hennen, M., Hollermann, D.E., Bardow, A., 2020. DeLoop: decomposition-based long-term operational optimization of energy systems with time-coupling constraints. Energy 198, 117272. doi:10.1016/j.energy.2020.117272.

Bischi, A., Taccari, L., Martelli, E., Amaldi, E., Manzolini, G., Silva, P., Campanari, S., Macchi, E., 2019. A rolling-horizon optimization algorithm for the long term operational scheduling of cogeneration systems. Energy 184, 73–90. doi:10.1016/j.energy.2017.12.022.

Chen, Z., Avraamidou, S., Liu, P., Li, Z., Ni, W., Pistikopoulos, E.N., 2021. Optimal design of integrated urban energy systems under uncertainty and sustainability requirements. Comput. Chem. Eng. 155. doi:10.1016/J.COMPCHEMENG.2021.107502.

Čuček, L., Martín, M., Grossmann, I.E., Kravanja, Z., 2014. Multi-period synthesis of optimally integrated biomass and bioenergy supply network. Comput. Chem. Eng. 66, 57–70. doi:10.1016/J.COMPCHEMENG.2014.02.020.

De Soto, W., Klein, S., Beckman, W., 2006. Improvement and validation of a model for photovoltaic array performance. Sol. Energy 80 (1), 78–88. doi:10.1016/j.solener.2005.06.010.

Fazlollahi, S., Bungener, S.L., Mandel, P., Becker, G., Maréchal, F., 2014. Multi-objectives, multi-period optimization of district energy systems: I. Selection of typical operating periods. Comput. Chem. Eng. 65, 54–66. doi:10.1016/j.compchemeng.2014.03.005.

Gabrielli, P., Gazzani, M., Martelli, E., Mazzotti, M., 2018. Optimal design of multi-energy systems with seasonal storage. Appl. Energy 219, 408–424. doi:10.1016/j.apenergy.2017.07.142.

Gabrielli, P., Gazzani, M., Mazzotti, M., 2018. Electrochemical conversion technologies for optimal design of decentralized multi-energy systems: modeling framework and technology assessment. Appl. Energy 221, 557–575. doi:10.1016/j.apenergy.2018.03.149.

Gabrielli, P., Poluzzi, A., Kramer, G.J., Spiers, C., Mazzotti, M., Gazzani, M., 2020. Seasonal energy storage for zero-emissions multi-energy systems via underground hydrogen storage. Renew. Sustain. Energy Rev. 121, 109629.

Geidl, M., Koeppel, G., Favre-Perrod, P., Klöckl, B., Andersson, G., Fröhlich, K., 2007. Energy hubs for the future. IEEE Power Energy Mag. 5 (1), 24–30. doi:10.1109/MPAE.2007.264850.

Grossmann, I.E., Apap, R.M., Calfa, B.A., Garcia-Herreros, P., Zhang, Q., 2015. Recent advances in mathematical programming techniques for the optimization of process systems under uncertainty. Comput. Aided Chem. Eng. 37, 1–14. doi:10.1016/B978-0-444-63578-5.50001-3.

Gurobi Optimization LLC, 2000. Gurobi, version 9.1.

Jerez, S., Thais, F., Tobin, I., Wild, M., Colette, A., Yiou, P., Vautard, R., 2015. The CLIMIX model: a tool to create and evaluate spatially-resolved scenarios of photovoltaic and wind power development. 10.1016/j.rser.2014.09.041.

Kotzur, L., Markewitz, P., Robinius, M., Stolten, D., 2018. Impact of different time series aggregation methods on optimal energy system design. Renew. Energy 117, 474–487. doi:10.1016/j.renene.2017.10.017.

Kotzur, L., Markewitz, P., Robinius, M., Stolten, D., 2018. Time series aggregation for energy system design: modeling seasonal storage. Appl. Energy 213, 123–135. doi:10.1016/j.apenergy.2018.01.023.

Löfberg, J., 2004. YALMIP: a toolbox for modeling and optimization in MATLAB. In: Proceedings of the IEEE International Symposium on Computer-Aided Control System Design, pp. 284–289. doi:10.1109/cacsd.2004.1393890.

Marquant, J.F., Evins, R., Carmeliet, J., 2015. Reducing computation time with a rolling horizon approach applied to a MILP formulation of multiple urban energy hub system. In: Procedia Computer Science. Elsevier B.V., pp. 2137–2146. doi:10.1016/j.procs.2015.05.486.

Mitra, S., Grossmann, I.E., Pinto, J.M., Arora, N., 2012. Optimal production planning under time-sensitive electricity prices for continuous power-intensive processes. Comput. Chem. Eng. 38, 171–184. doi:10.1016/J.COMPCHEMENG.2011.09.019.

Nahmmacher, P., Schmid, E., Hirth, L., Knopf, B., 2016. Carpe diem: a novel approach to select representative days for long-term power system modeling. Energy 112, 430–442. doi:10.1016/j.energy.2016.06.081.

Peng, X., Bajaj, I., Yao, M., Maravelias, C.T., 2021. Solid-gas thermochemical energy storage strategies for concentrating solar power: optimization and system analysis. Energy Convers. Manage. 245. doi:10.1016/j.enconman.2021.114636.

Pfenninger, S., 2017. Dealing with multiple decades of hourly wind and PV time series in energy models: a comparison of methods to reduce time resolution and the planning implications of inter-annual variability. Appl. Energy 197, 1–13. doi:10.1016/j.apenergy.2017.03.051.

Pilpola, S., Lund, P.D., 2020. Analyzing the effects of uncertainties on the modelling of low-carbon energy system pathways. Energy 201. doi:10.1016/J.ENERGY.2020.117652.

Priesmann, J., Nolting, L., Praktiknjo, A., 2019. Are complex energy system models more accurate? An intra-model comparison of power system optimization models. Appl. Energy 255, 113783. doi:10.1016/j.apenergy.2019.113783.

Samsatli, S., Samsatli, N.J., 2018. A multi-objective MILP model for the design and operation of future integrated multi-vector energy networks capturing detailed spatio-temporal dependencies. Appl. Energy 220, 893–920. doi:10.1016/j.apenergy.2017.09.055.

Schütz, T., Schraven, M.H., Fuchs, M., Remmen, P., Müller, D., 2018. Comparison of clustering algorithms for the selection of typical demand days for energy system synthesis. Renew. Energy 129, 570–582. doi:10.1016/j.renene.2018.06.028.

Teichgraeber, H., Lindenmeyer, C.P., Baumgärtner, N., Kotzur, L., Stolten, D., Robinius, M., Bardow, A., Brandt, A.R., 2020. Extreme events in time series aggregation: a case study for optimal residential energy supply systems. Appl. Energy 275, 115223. doi:10.1016/j.apenergy.2020.115223.

The MathWorks Inc., 2018. MATLAB, version 9.4 (R2018a).

Tso, W.W., Demirhan, C.D., Heuberger, C.F., Powell, J.B., Pistikopoulos, E.N., 2020. A hierarchical clustering decomposition algorithm for optimizing renewable power systems with storage. Appl. Energy 270, 115190. doi:10.1016/J.APENERGY.2020.115190.

Vom Stein, D., Van Bracht, N., Maaz, A., Moser, A., 2017. Development of adaptive time patterns for multi-dimensional power system simulations. In: 2017 14th International Conference on the European Energy Market (EEM) doi:10.1109/EEM.2017.7981868.

Weimann, L., Ellerker, M., Kramer, G.J., Gazzani, M., 2019. Modeling gas turbines in multi-energy systems: a linear model accounting for part-load operation, fuel, temperature, and sizing effects. In: International Conference on Applied Energy.

Weimann, L., Gabrielli, P., Boldrini, A., Kramer, G.J., Gazzani, M., 2021. Optimal hydrogen production in a wind-dominated zero-emission energy system. Adv. Appl. Energy 100032. doi:10.1016/j.adapen.2021.100032.

Wirtz, M., Hahn, M., Schreiber, T., Müller, D., 2021. Design optimization of multi-energy systems using mixed-integer linear programming: which model complexity and level of detail is sufficient? Energy Convers. Manage. 240, 114249. doi:10.1016/j.enconman.2021.114249.

Zatti, M., Gabba, M., Freschini, M., Rossi, M., Gambarotta, A., Morini, M., Martelli, E., 2019. k-MILP: a novel clustering approach to select typical and extreme days for multi-energy systems design optimization. Energy 181, 1051–1063. doi:10.1016/j.energy.2019.05.044.

Zhang, Q., Martín, M., Grossmann, I.E., 2019. Integrated design and operation of renewables-based fuels and power production networks. Comput. Chem. Eng. 122, 80–92. doi:10.1016/j.compchemeng.2018.06.018.